DYNAMICS OF WAVE BREAKING AT A COASTAL SEA WALL

A Thesis

by

ARTHUR L.C. ANTOINE

Submitted to the Office of Graduate Studies of
Texas A&M University
in partial fulfillment of the requirements for the degree of

MASTER OF SCIENCE

December 2009

Major Subject: Ocean Engineering

DYNAMICS OF WAVE BREAKING AT A COASTAL SEA WALL

A Thesis

by

ARTHUR L.C. ANTOINE

Submitted to the Office of Graduate Studies of
Texas A&M University
in partial fulfillment of the requirements for the degree of

MASTER OF SCIENCE

Approved by:

Chair of Committee,	Kuang-An Chang
Committee Members,	James Kaihatu
	Chin B. Su
Head of Department,	John Niedzwecki

December 2009

Major Subject: Ocean Engineering

ABSTRACT

Dynamics of Wave Breaking at a Coastal Sea Wall.

(December 2009)

Arthur L.C. Antoine, B.S., University of the West Indies

Chair of Advisory Committee: Dr. Kuang-An Chang

Structural designs barely consider the dynamic scenario of a well-developed impinging wave hitting the structure. The usual area of focus is on static and stability factors (e.g. drag, inertia, resistive forces related to weight, buoyancy, sliding etc). Even the "Factor of Safety" which is regularly used in designs to account for unknown and/or unforeseen situations which might occur implies a degree of uncertainty about the dynamic scenario of breaking waves in the coastal environment.

In the present study the hydrodynamics of a coastal structure-turbulent bore interaction was studied by examination (two-dimensional) of the singular case of a plunging breaking wave forming a well developed turbulent bore which impacted on a model sea wall structure.

The turbulent bore impact event was found to display similar characteristics to the impact event of other wave shapes, in particular that of a plunging breaker. Examination of the impact event confirmed the conversion of nearly all horizontal velocity to vertical velocity during the "flip through" event.

In accordance with theoretical expectations the location of maximum pressure was found to occur just below the still water level (SWL).

Resulting pressure data in the present study consisted of two blunt spikes as opposed to the "church-roof" (high spike) shape seen in other results. The shape of the pressure data was attributed to the following: firstly, to the initial impact of the protruding jet of the breaking wave which causes the first maxima, secondly, to the sensor encountering the bulk of the entrapped air hence causing the drop in pressure between the blunt spikes and lastly, to the inherent hydrostatic pressure combined with the compression of the entrapped air bubbles, by the subsequent forward motion of the water within the wave, which causes the second maxima. The point of maximum pressure was found to always be within the second maxima.

Observation of the turbulent bore-structure interaction showed that the consequential maximum pressure was a direct result of the compression of entrapped air by the weight of the water in the wave as it continued forward onto the structure combined with the inherent hydrostatic pressure of the wave.

The project was conducted in an attempt to contribute to the vast knowledge of coastal structure-wave interactions and to add to the understanding of the physics and characteristics of breaking waves. Whilst numerous studies and experiments have been carried out on the phenomenon of breaking waves by previous researchers the current project highlights the advent of new equipment and technological advances in existing methods.

Dedicated to my dear cousin Heather Clemens, neé Coppin.

ACKNOWLEDGMENTS

Grateful thanks go to my committee chair, committee members, my sponsor (OAS/LASPAU), intra/extra-departmental friends and colleagues, my parents and last, but not least, to the TAMU and TEES staff for their assistance, guidance and support throughout the course of this research.

NOMENCLATURE

BIV	Bubble Image Velocimetry
PIV	Particle Image Velocimetry
PC	Personal Computer
h.o.w.	Head of Water
DAQ	Data Acquisition
SWL	Still Water Level

TABLE OF CONTENTS

CHAPTER Page

LIST OF FIGURES

FIGURE Page

LIST OF TABLES

CHAPTER I

INTRODUCTION

Sea walls background

Sea walls are usually on shore structures along the coastline that serve to protect the landward area against severe damage from wave action; damage such as flooding due to storm surge and erosion. For various reasons they tend to be the most popular selected form of structural protection. In highly populated or visited areas such as tourist sites they lend themselves to the recreational purpose or functional use of the area by providing accessible space at the top of the wall.

In many (small) island states where there may be limited space or other constraining factors sea walls are often built in the water right up against the shoreline. In such cases it is common to find a roadway and/or pedestrian thoroughfare at the top of the wall.

Though the majority of sea walls in application may be vertical or close to vertical it is not uncommon to find a variety of designs incorporating different features and constructed of different materials. For instance curved seawalls serve to redirect

---

This thesis follows the style of Coastal Engineering.

waves out to sea thus reducing the amount of overtopping. Sloped and/or stepped sea walls help to dissipate wave energy as the wave runs up the sloping face of the wall which may be stepped to further reduce the energy of the wave.

Regardless of form or shape the main feature of any typical sea wall is to effectively or rather immediately dissipate the energy of oncoming waves while remaining structurally sound.

Literature review and present status of the subject

Structural designs barely consider the dynamic scenario of a well-developed impinging wave hitting the structure. The usual area of focus is on static and stability factors (e.g. drag, inertia, resistive forces related to weight, buoyancy, sliding etc). Even the "Factor of Safety" which is regularly used in designs to account for unknown and/or unforeseen situations that might occur implies a degree of uncertainty about the dynamic scenario of breaking waves in the coastal environment.

The processes involved in wave breaking, namely shoaling and loss of energy to bottom friction, have been well established theoretically and practically. However, though the dynamics of coastal waves has long been an interesting study topic in Coastal Engineering the issue remains unsettled.

There have been numerous studies and experiments on the topic both practical and numerical; dating as far back to the novel findings of Minikin (1963) who may have been the first to establish that a coastal structure would not experience any shock

pressure unless the impinging wave had trapped some amount of air, to the crafty efforts of Kamel (1970) with the efforts of his "plate drop" experiment as detailed in his publication.

Over the years, with advances in technology, experimental and numerical methods there has been continuous variation in the findings of researchers in relation to the dynamics of breaking waves in the coastal environment.

Initially the dynamic parameters of the wave (namely pressure and velocity) were classified based on wave type or rather the shape of the wave. Hull and Muller (2002) presented interesting findings from an experiment that focused on various wave shapes and the resulting impact pressures. Lugni et al. (2006) suggested that "the shape of the impacting wave has a significant effect on wave impact pressure exerted on vertical walls." The trend in researchers' perspectives has shifted from this form of classification to more in-depth focus on the dynamic wave parameters. More detailed focus has been made possible by advances in technology.

Hattori and Arami (1992) made mention of the difficulty in measuring "the change of the entrapped air amount due to the irregularity of the wave front". Many researchers appreciate the importance of recording this phenomenon however efforts are still being made towards accurate and consistent recording methods.

Many previous researchers, including Schmidt et al. (1992), Hattori and Arami (1992), Hattori et al. (1994), Peregrine and Topliss (1994), Kirkgöz (1995), Bullock et al. (2001), Lugni et al. (2006) and Bullock et al. (2007), have made attempts at

observing the influence of the air entrapped by a breaking wave impinging on some form of structure.

Hitherto, the most used method, as was done by Hattori et al. (1994), Kirkgöz (1995) and Lugni et al. (2006), has been by visually quantifying the spatial amount of the entrapped air at the moment the wave impinges on the structure; termed the "thickness" of the air pocket by these researchers.

Schmidt et al. (1992) provided a unique means of obtaining the elusive measurement from sound velocity. Peregrine and Topliss (1994) introduced a numerical method for the singular case of a wave entrapping a single air pocket or single bubble.

Bullock et al. (2001) and Bullock et al. (2007) incorporated pressure aeration units (PAUs) which were devices used to simultaneously measure pressure and the level of aeration (i.e. void ratio) of the impinging wave. These PAUs were of significant size to interfere with the dynamics of the wave. In addition, the void ratio which was "estimated from Maxwell's equation (Maxwell, 1892) by measuring the conductivity of the fluid between two vertical stainless steel electrodes" was considered as "indicative rather than precise" as a result of the inherent flaws of the method (detailed in the 2007 publication). Further specifics of the instrumentation can be found in Bird et al. (1998).

The numerous publications on the dynamics of breaking waves at the coast all present various, at times contradicting, results especially in relation to the effect of the air entrapped by the breaking wave.

Blackmore and Hewson (1984), Hattori and Arami (1992), Hattori et al. (1994) and Kirkgöz (1995) all presented results supporting the notion that maximum shock

pressures were induced on a coastal structure in the absence of entrapped air. They claimed that the presence of air in the impinging wave reduced the pressure by providing a "cushioning" effect.

Whillock (1987), Bullock et al. (2001) and Bullock et al. (2007) presented conflicting results that the maximum pressures were experienced with the presence of entrapped air. These researchers attributed the high shock pressures experienced to the "compression" of the entrapped air pocket by the trailing body of water in the wave.

An exceptional observation was presented by Peregrine (2003) and Lugni et al. (2006) which suggested the high pressure occurring at a sea wall was as a result of the acceleration of a vertical jet of water which was formed when the wave experienced a "flip-through" event.

Regardless of the diverse perspectives relating to the amount of air within the impinging wave a common ground in all the researchers' results is that the amount of entrapped air is directly related to the trailing frequencies observed in recorded pressure data.

Generally, the trailing "frequencies of oscillations" subsequent to the initial shock pressure are "inversely proportional" to the amount of air entrapped by the impinging wave (Peregrine et al. 1992).

The present research studies the hydrodynamics of a turbulent bore-structure interaction in an attempt to contribute to the vast knowledge of coastal structure-wave interactions. The experiment focuses on the singular case of a plunging breaking wave forming a well developed turbulent bore impacting on a model sea wall structure.

The breaking wave condition used in this experiment presents a more realistic scenario than the idealized case in which the breaking wave impinges directly onto the structure face. The latter case, though not impossible, would be a rarity in actual application because of the inherent effects of location, topography/bathymetry, structural design of the wall (e.g. stepped/sloped, toe protection etc.) and the usual high reflection of wave energy at sea walls which would affect incoming waves.

Thesis overview

Bubble image velocimetry, an innovative and recently developed technique, was used to obtain velocity field data. Ryu et al. (2005) and Ryu (2006) provide explicit descriptions of the technique. Essentially, the BIV technique involved the observation of the experiment with a high-speed video camera for capturing the motion of the breaking wave on the structure and specific software for analysis of the images obtained.

Pressure data acquisition was accomplished by the use of piezo-resistive relative pressure sensors (type 4053A) from Kistler.

The breaking wave was generated by a wave focusing method that consisted of a train of waves of varying frequencies (as in Ryu 2006). This technique was facilitated by use of the Civil Laboratory wave tank of the Zachry Department of Civil Engineering at Texas A&M University.

A description of the experiment set-up used, hardware, measurement methods, data acquisition techniques and processing is presented in Chapter II. Chapter III

includes a discussion of the results in light of specific limitations. In Chapter IV the study presents an explicit account of the possibilities for future work.

CHAPTER II

EXPERIMENT SET-UP

Overview of experiment set-up and measurement methods

The model structure was designed for use in the Civil Laboratory wave tank of the Texas A&M University. The model simulated a typically constructed vertical sea wall in application and was constructed of in the Nuclear Engineering Workshop of the Texas A&M University.

The wave tank dimensions are 0.91 m width by 1.22 m depth and it measures 37 m in length. At the opposite end to the flap type wave maker the tank is fitted with a beach slope (1:5.5) covered with horsehair to reduce reflection of wave energy in the tank.

The selection of a vertical sea wall as the model structure aided the objective of attaining direct measurements of the dynamic parameters of the wave.

The model structure was positioned 18.7 m away from the wave maker. The width of the model structure (0.90 m) allowed it to fit flush with the wave tank side walls. Silicone was used to seal the remaining small gap as water passing through the space would have been recorded by the camera which was used for the BIV process; also, the velocity of the water in this location would have been irrelevant. Figure 2.1 presents a section view showing the model structure details and dimensions along with

the FOV used for the experiment. The model scale was 1/10 (correlating to a typical coastal sea wall with a 2 m freeboard above SWL).

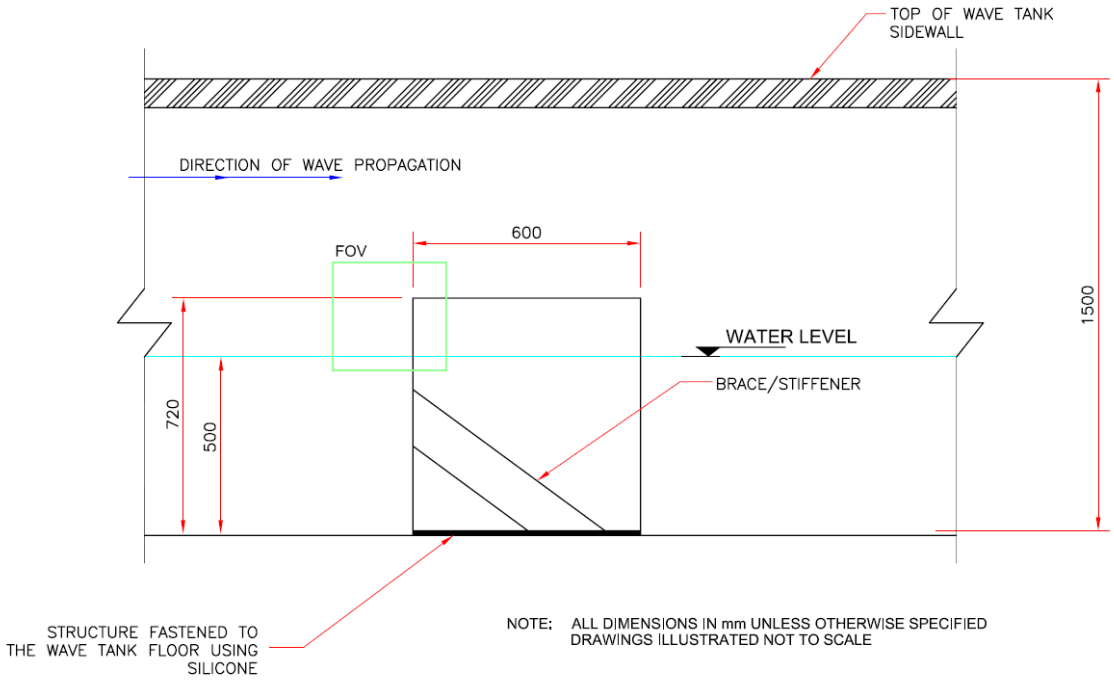

Figure 2.1 Model structure details.

The arrangement facilitated a two-dimensional perspective of the experiment with the camera set up to the side of the structure viewing through the glass of the wave tank. Ignoring the many complexities of sea walls in coastal applications such as variation of the depth of water at the wall and topography effects the experiment focused on the simplified scenario of an adequately designed wall with a smooth, vertical front face on a horizontal sea bed. Figure 2.2 shows the actual experiment set up.

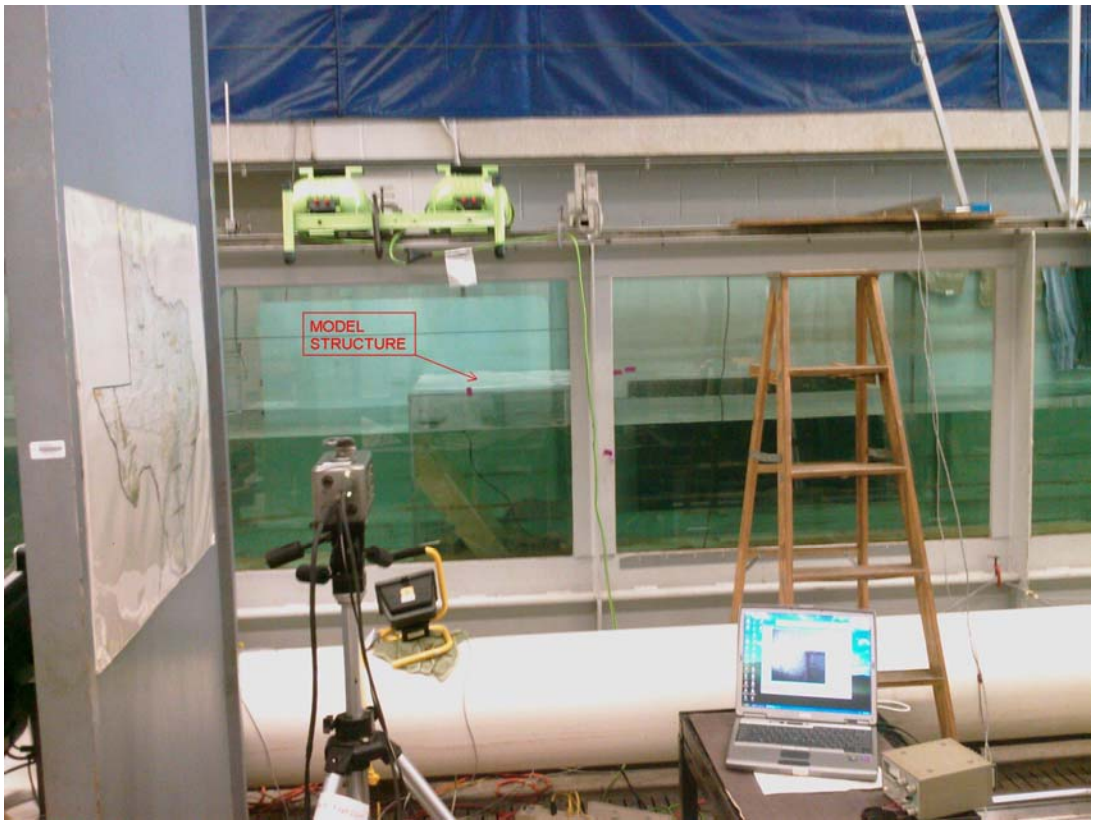

Figure 2.2 Actual experiment set up.

A single Field Of View (FOV) (43 cm x 43 cm) was used to observe and record the experiment in the vicinity of the upper front area of the model structure.

The wave conditions used in the wave tank were selected based on similar wave conditions experienced at the location of vertical sea walls in coastal applications.

The experiment focused on the singular case of a breaking wave with the following characteristics: T = 1.1s, H = 9.6cm and C = 2.2 m/s. The intermediate water depth ($\pi/10 < kh < \pi$; as per Dean and Dalrymple (1992)) of 50cm was kept constant throughout the experiment.

Consider the schematic shown in figure 2.3 which illustrates a wave impinging on a typical vertical sea wall. It was imperative to be able to quantify the impact pressures occurring on the model structure during the experiment. Kistler pressure sensors were used on the front face of the model structure for (spatial and temporal) measurement of the impact pressure. The breaking wave condition used in this experiment presents a more realistic scenario than the idealized case in which the breaking wave impinges directly onto the structure face. The latter case, though not impossible, would be a rarity in actual application because of the inherent effects of location, topography/bathymetry, structural design of the wall (e.g. stepped/sloped, toe protection etc.) and the usual high reflection of wave energy at sea walls which would affect incoming waves.

Knowledge of the velocities associated with such an impinging wave was also vital. Particle Imaging Velocimetry (PIV) or rather Bubble Imaging Velocimetry (BIV), a variation of the former, was used for velocity measurement.

BIV involved the observation of the experiment with a high speed video camera for capturing the motion of the breaking wave on the structure and associated software for analysis of the images obtained.

Mean velocity data was calculated as per Ryu (2006) by ensemble averaging of the measured instantaneous velocities at each phase. In this case for mean velocity a total of thirty test waves (N = 30) provided the instantaneous velocity measurements.

Mean pressure data was obtained from the ensemble averaging of the data from ten test waves for three different locations of interest while simultaneously recording

each test wave with the camera which resulted in a minimum of thirty test cases for obtaining the mean velocity field data from the BIV process.

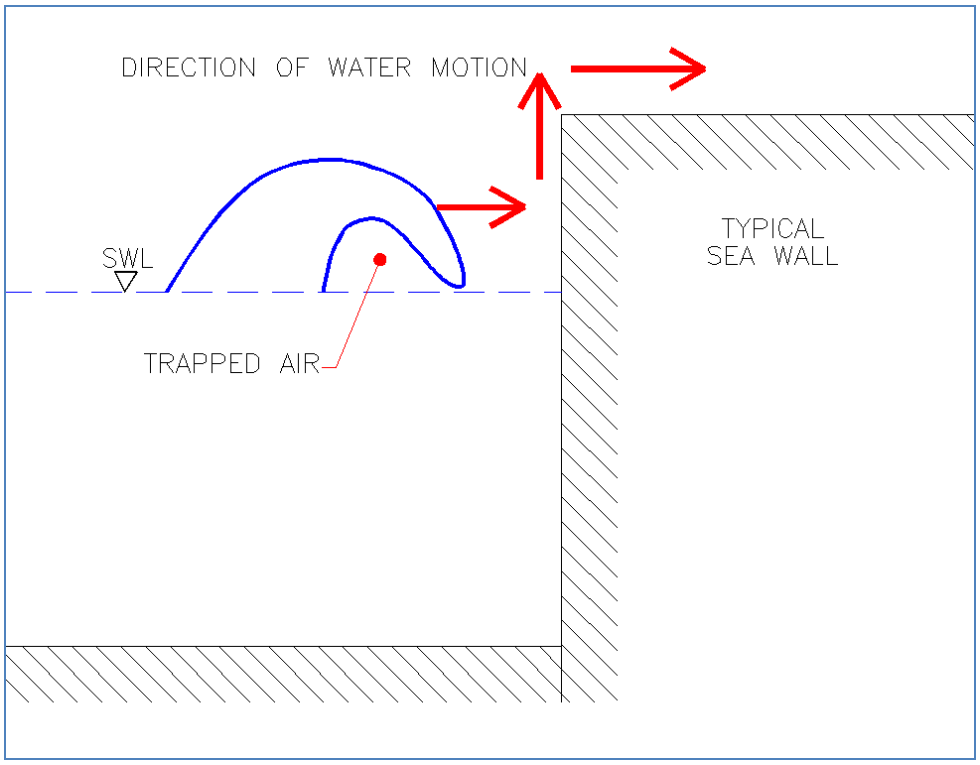

Figure 2.3 Impinging wave schematic.

Wave maker and wave generation

The experiment was conducted in the Civil Laboratory wave tank of the Zachry Department of Civil Engineering at Texas A&M University. The tank and wave generation system essentially composed of "a Sea Sim Rolling Seal absorbing Wave maker (RSW 90-85), a dry back, aluminum space frame, and PVC cased, modular,

hinged flap wave maker. The flap is sealed by a low friction rolling seal and is driven by a precision, electronically commutated synchronous servomotor, while being hydrostatically balanced using an automatic near constant force, pneumatic control system" (Sea Sim Rolling Seal Absorbing Wave maker Manual, Data sheet RSW 382).

The wave maker was operated by a computer equipped with a National Instruments AT-MIO-16E-2 data acquisition board and an in-house developed National Instruments LabVIEW program.

Waves were generated by a DC voltage analog output signal which was created by the in-house developed National Instruments LabVIEW program that also served as the signal driver for BIV, pressure and other laboratory hardware. This set-up accommodated the precise synchronization of data acquisition for the experiment.

The breaking wave was generated by a wave focusing method that consisted of a train of waves of varying frequencies and amplitudes. Essentially the wave focusing method generates both short and long waves (in that order); the faster moving long waves catch up to the slower moving short waves at a desired location to form the breaking wave. The characteristics of the breaking wave and the point of breaking were controlled by modification of the software input parameters in the LabVIEW signal driver program. Figure 2.4 shows the progression of the wave onto the structure.

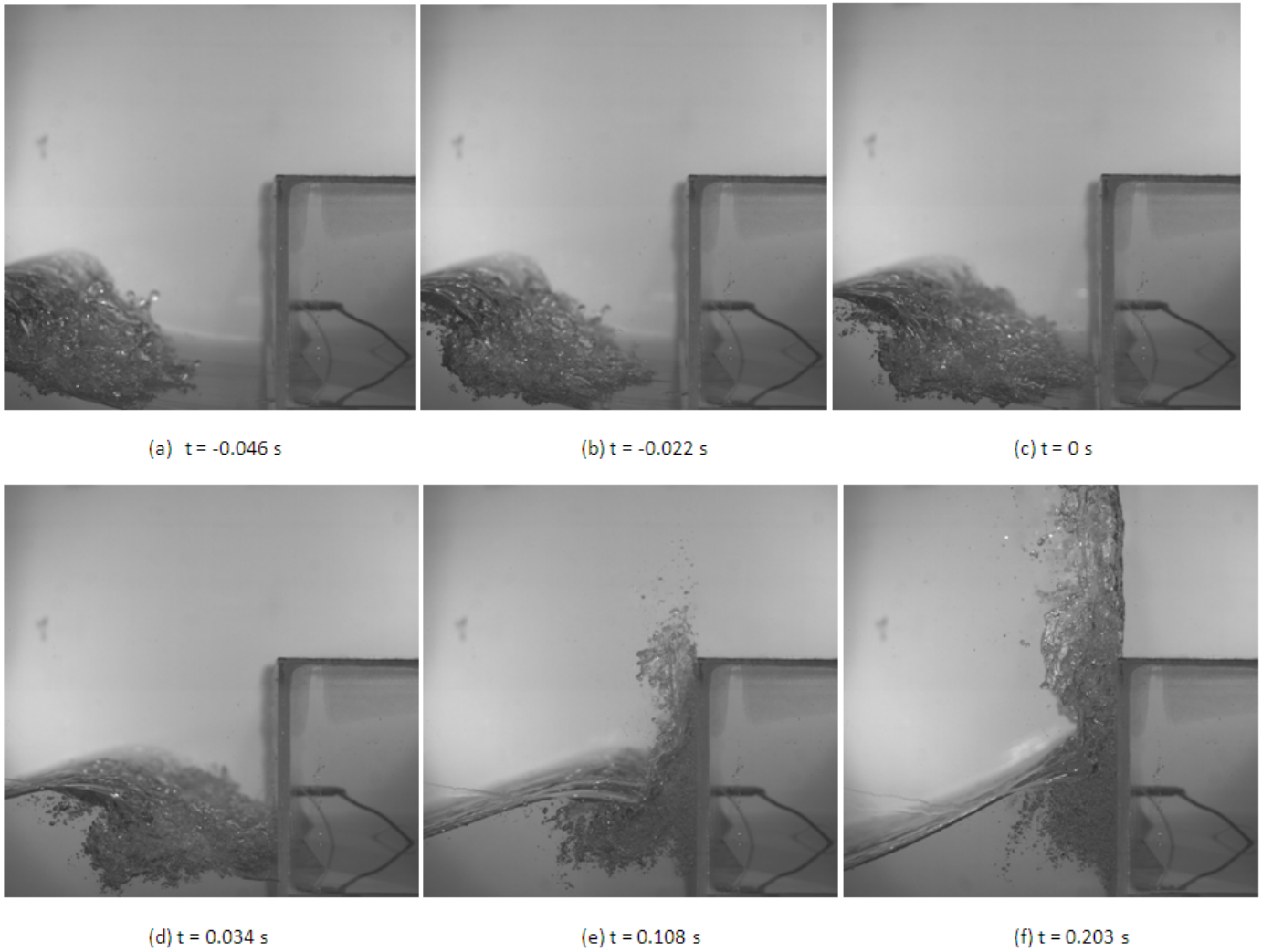

Figure 2.4 Breaking wave progression.

The instant when the leading edge of the wave made contact with the front wall of the structure was defined as t = 0 s. All instantaneous data (pressure, velocity and BIV movies) were matched to this moment.

It should be mentioned that during the setting up of the experiment (by variation of the input signal), a standing wave phenomenon could be witnessed and occurred frequently between the structure and wave maker. Wave energy reflection significantly affected the attainment of the desired wave maker signal, in particular during the initial set up period for the experiment. The inherent high wave energy reflection was expected as a consequence of the flat, smooth, vertical front face of the model structure and the structure's orientation within the wave tank.

In order to ascertain the wave characteristics, wave elevation data was measured and recorded by using double-wire resistance-type wave gauges at required locations. These gauges are effective at recording water level data especially in non-aerated situations because they measure the total length ("wet length") of the double-wire which is in contact with the water at any point in time.

The wave elevation data was recorded by a separate computer which was also equipped with another National Instruments data acquisition board along with in-house developed National Instruments LabVIEW software.

With the equipment (wave maker and wave gauges) synchronized the time of impact of the impinging breaking wave at the model structure was known. Hence the particular breaking wave could then be identified on a plot of the wave elevation data. The data was recorded at a sample rate of 25 Hz for duration of 100 seconds for a

minimum of three trials then it was averaged in order to ascertain the wave characteristics. Furthermore, as per Ryu and Chang (2008), "the primary wave period obtained by zero up-crossing, was the period of the specific wave in the wave train which had the largest wave amplitude and lead to the breaking event."

To ensure repeatability of the test waves and for proper data recording the water in the wave tank was allowed to settle for at least fifteen minutes between each test wave. The absorption feature of the wave maker proved to be quite useful in this regard. The wave maker was equipped with a built-in on/off switch that facilitated the use of the absorption feature between test waves. Figure 2.5 illustrates the complete experimental set-up.

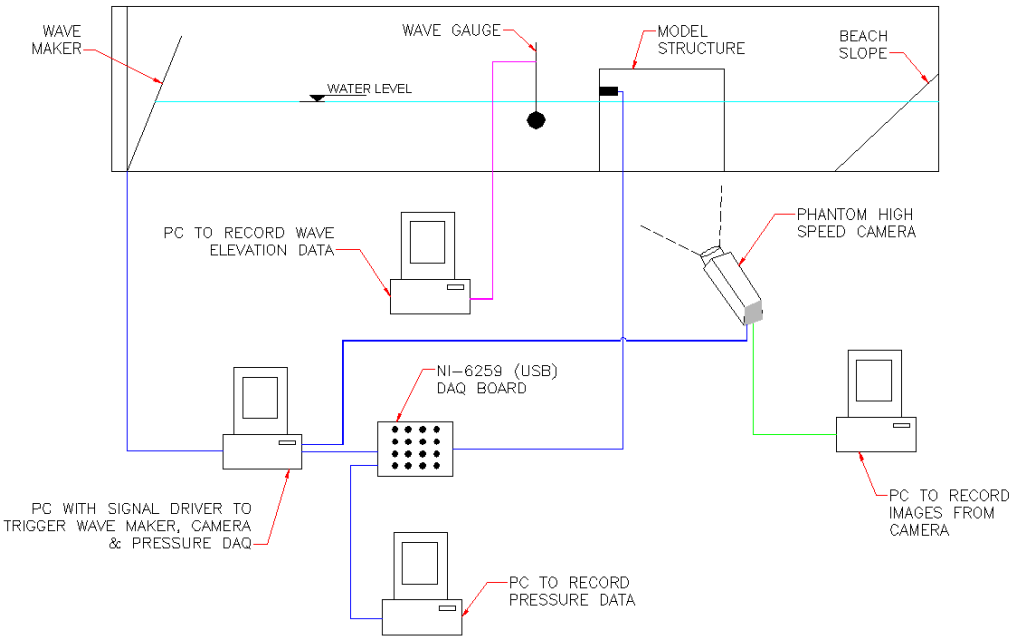

Figure 2.5 Experiment set-up.

Bubble image velocimetry technique

Knowledge of the velocities associated with the impinging wave is vital. Bubble Imaging Velocimetry (BIV) a variation of the Particle Imaging Velocimetry (PIV) technique was used for velocity measurement.

Since the initial development of the techniques their advantage and efficiency for velocity measurement have been well established and validated by several researchers. A major advantage of BIV and PIV is that they are visual methods and hence provide a completely non-intrusive means of obtaining velocity field data. Work done by Ryu et al. (2005), Ryu and Chang (2008) and Seol et al. (2007) are some informative publications detailing these techniques.

The main difference between the two techniques for velocity measurement is that with PIV, seeding particles of neutral buoyancy are required within the flow under consideration. These seeding particles are then illuminated, usually by a laser, as their motion is captured by a camera whereas "BIV uses bubbles and air-water interfaces as tracers" (Ryu and Chang 2008).

Essentially, the BIV technique involved the observation of the experiment with a high speed video camera for capturing the motion of the breaking wave on the structure and specific software for analysis of the images obtained.

Image recording for BIV

A Phantom v5.1 high speed video camera (from Vision Research) and the accompanying camera control software (Phantom 630.A v8.4) were used to record the motion of the breaking wave.

A single Field Of View (FOV) (43 cm x 43 cm) was used to observe the breaking wave in the vicinity of the upper front area of the model structure. This FOV was adequate to capture the motion of the wave as it hit the structure and the subsequent motion of the water after impinging.

The camera was set up a distance of 1.47 m away from the glass wall of the wave tank and at a height of 1.35 m.

Similar to the set-up of Ryu and Chang (2008) the flow was illuminated by a shadowgraphy technique with light from the back of the wave tank. Two 600 watt halogen lamps were set up to the back of the wave tank, one to each side of the FOV area focusing on the area at a slight angle, the lamps shone through a white (translucent) acrylic sheet which was fastened to the back glass wall of the wave tank in order to spread the light source. Preliminary trial processing of the images obtained with this lighting set-up indicated that additional lighting was required to improve the quality of the BIV results.

Additional lighting used included a professional grade twin head halogen work lamp set and a pair of 500 watt halogen work lamps. The twin head halogen work lamp set comprised of a 250 watt and 500 watt bulb for 750 watts per housing totaling 1500

watts. This lamp set was fixed to the top of the wave tank aiming downwards onto the FOV area at an angle of about 45 degrees. The pair of 500 watt halogen work lamps was set up at the front of the wave tank, one to each side of the FOV area focusing on the area at a slight angle. Figure 2.6 shows a sample of the results with adequate lighting.

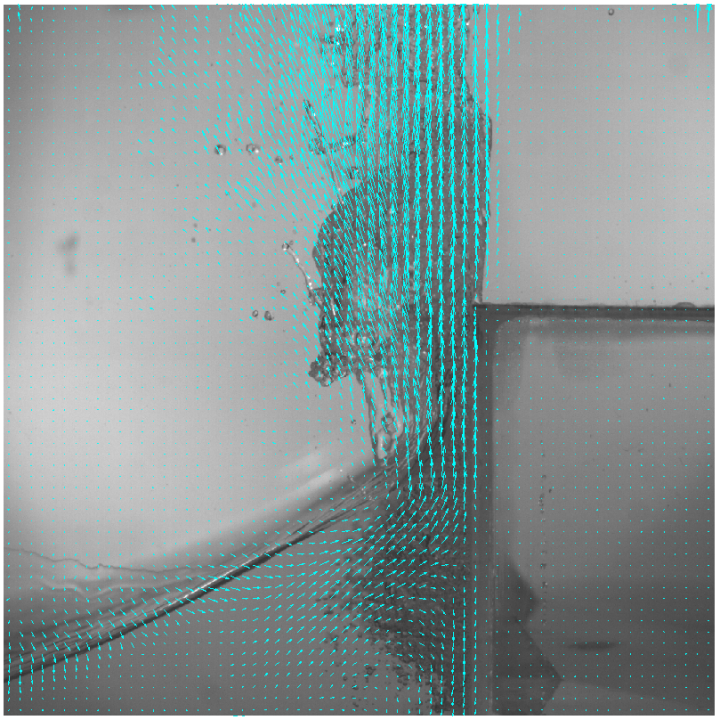

Figure 2.6 Sample of BIV results with proper lighting.

The image captured by the camera was continually checked during the setting up of the final lighting arrangement to ensure that there was no significant reflection of light by the water since light reflection would adversely affect the BIV results.

The Phantom v5.1 is an 8-bit digital high speed video camera with a maximum sampling (framing) rate of 1000 frames per second and a maximum resolution of 1024 x

1024 pixels. The camera was fitted with a 60 mm focal lens which was set to the lowest aperture size (f/2.8). The sampling rate used in the experiment was set in the Phantom 630.A software at 1000 frames per second (fps) with an exposure time of 400 micro-seconds.

Throughout the experiment the camera was kept focused at a point exactly 15 cm into the wave tank, away from the front glass wall. This point can be referred to as the center of the camera's focal plane or center of the depth of field (DOF). According to Ryu (2006) this location (15 cm into the tank) was sufficiently far away form the front glass wall for boundary effects to be insignificant.

The DOF is essentially a thin area within which objects or motion captured by the camera appears sharp and well focused. Following Ryu (2006) the size of the DOF for the experiment was found to be 0.13 m, calculated using the following equation, DOF = S – R; in which S is the farthest limit and R the nearest limit of the DOF. S and R were calculated as follows $S = Lf^2(f^2 - NLC)$ and $R = Lf^2(f^2 + NLC)$; in which L is the distance between the focal plane and camera (1.64 m), f is the focal length of the camera lens (60 mm), N the f-number of the camera aperture (f/2.8) and C a constant value which was a property of the camera used (0.03 mm). The error in the resulting velocity as a result of the size or thickness of the DOF was calculated to be 3.8% using the equation, error = DOF/2L.

The camera was connected to receive the trigger signal directly from the aforementioned National Instruments AT-MIO-16E-2 DAQ board. This trigger signal created by the LabVIEW signal driver program, which also triggered the wave maker

and pressure data acquisition hardware, started the motion capture of the breaking wave at the required time.

BIV image processing

The movies acquired from the camera for each test wave were of approximately 2 s duration and were stored in *.cine format (minimum file size 2 GB).

Each of the acquired movies was then separated into (*.tif) image files (one image for each frame) using the Phantom 630.A software; their full duration of 2 s each with a framing rate of 1000 fps (equal to a 1 ms time difference between each frame) resulted in a minimum of 2000 images per movie.

The images were obtained in numerical sequence from the start to end of each movie. The acquired images were then coupled, with the succeeding image (that is image 1 and image 2, then image 2 and image 3 etc.), to form a single bitmap image which was then inverted (visually) so that dark low intensity areas in the original image would become bright high intensity areas. The inverting of the images aided the quality of the calculated velocity vectors from the BIV analysis by improving the (light) intensity variation which better revealed the bubble structure for correlation of the consecutive images. Figure 2.7 shows a sample of the original image and figure 2.8 shows a sample of the coupled and inverted image.

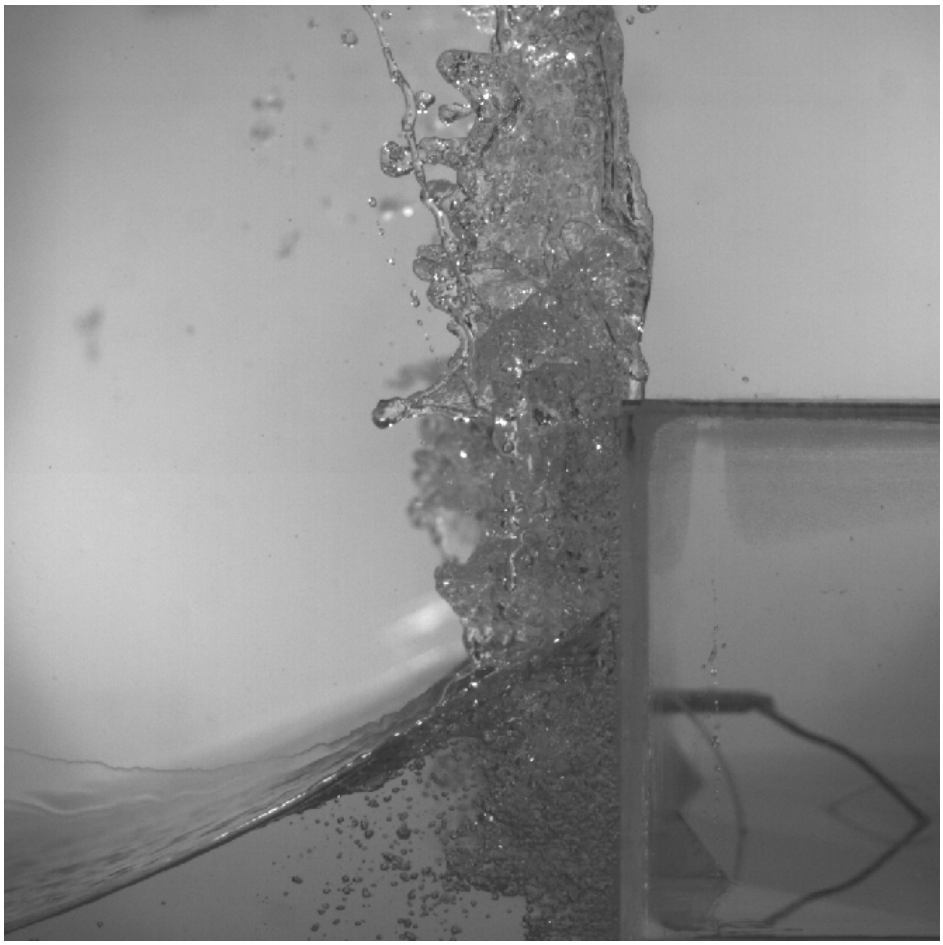

Figure 2.7 Original image.

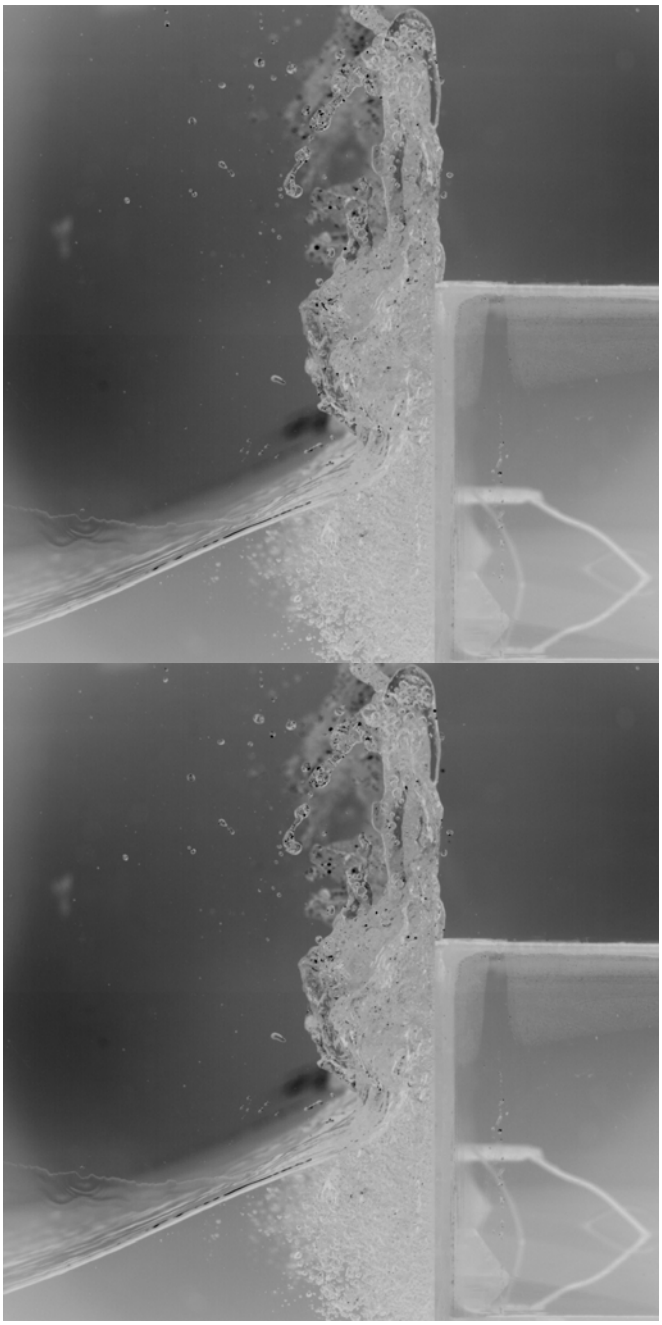

Figure 2.8 Coupled and inverted image for BIV analysis.

The consecutive coupled and inverted images were then processed using the Davis v6.2 program from LaVision Inc. which output the required velocity vectors for

the FOV for the movie duration. The Davis (LaVision Inc.) program was set to compute the velocity field data by a cross-correlation method with a 50% overlap between subsequent windows for an interrogation window size of 32 x 32 pixels.

Plotting the instantaneous velocity data from the Davis (LaVision Inc.) program, which was output in ascii format as text files, indicated that post-processing methods were necessary to improve the data quality by removal of spurious velocity vectors and vectors in irrelevant areas.

The MPIV manual along with the Matlab programming codes provided by Mori and Chang (2003) were used for post-processing of the images.

The post-processing method was as follows: spurious velocity vectors were removed by a median filter using the "mpiv_filter.m" code from the MPIV toolbox code set (available for download online, refer to Mori and Chang 2003), the instantaneous velocity data was ensemble averaged, removed vectors were replaced by interpolation using the same code "mpiv_filter.m", then the velocity data was processed using the "mpiv_smooth.m" code and finally the velocity vectors in irrelevant areas were removed by a masking technique which involved graphic manipulation of the original frame images of the breaking wave followed by correlation of these altered images with the velocity data (text files).

The final post-processed images were then compiled using the Phantom 630.A program to make a single movie which shows the velocity vectors for the entire motion of the breaking wave within the FOV (refer to Appendix A for the movies of the velocity data).

Pressure data acquisition

To be able to quantify the impact pressures occurring on the vertical wall during the experiment was of extreme importance. Piezo-resistive relative pressure sensors (type 4053A) from Kistler were used for (spatial and temporal) measurement of the impact pressure of the breaking wave.

Figure 2.9 shows the positions on the front face of the model structure at which pressure data was obtained from the experiment. It was ensured that the orientation of the sensor would be flush perpendicular to the surface during preparation of the front face of the model for fitting the sensor. The positions for the pressure sensors were arranged noting that a sparse distribution of the pressure sensors along the wall would be cause for lower values of the actual (maximum) pressure to be recorded (Lugni et al. 2006).

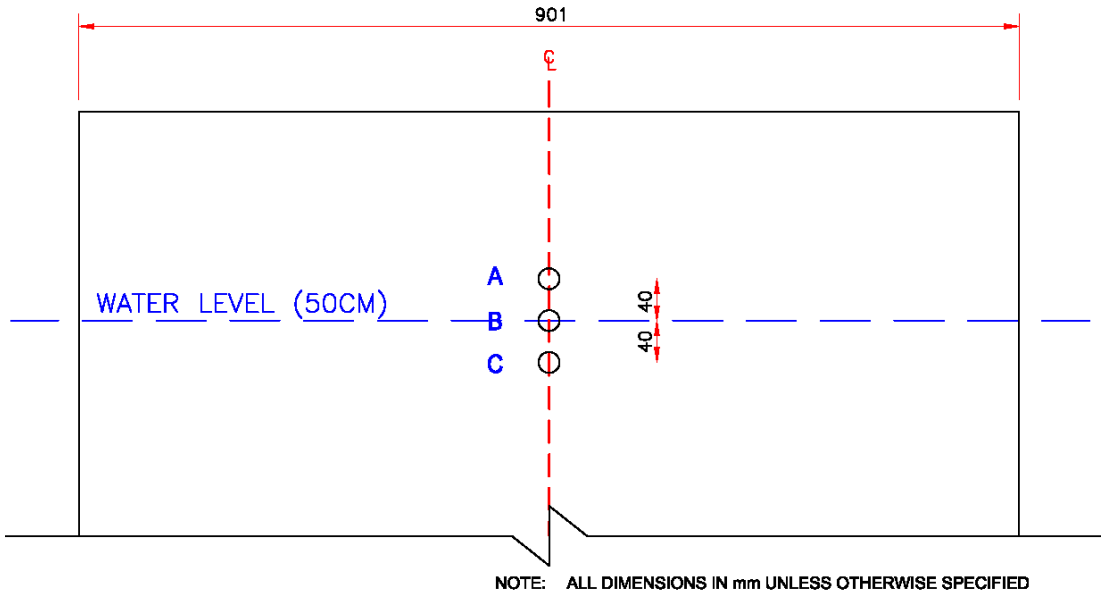

Figure 2.9 Pressure data positions.

According to the accompanying manufacturer's data sheet the selected pressure sensors are able to measure static and dynamic relative pressures and are distinguished by high output voltage, good linearity and stability together with small dimensions. They also allow for very dynamic measurements to be made as a result of their high natural frequency.

In addition, the sensors largely compensate for thermal effects; a key feature of the Kistler sensors which make them particularly applicable for research experimentation. The sensors compensate for thermal effects within the following temperature range: -20^{o}C to 50^{o}C (Kistler 4053A specifications data sheet). Initial trials using the sensors during the set-up of the experiment validated their thermal compensation feature.

The Kistler 4053A sensor manufacturer's data sheet provides an explicit description of the functioning of the sensor. The 4053A sensors are limited to pressure measurement up to 1 bar. Pressure measurement was made in relation to a reference pressure which in the case of the experiment was the local ambient (or atmospheric) pressure. This was facilitated by a hose attached to the reference pressure input of the sensor with the opposite end of the hose in air. Figure 2.10 shows an extract from the manufacturer's data sheet which details the dimensions of the pressure sensors.

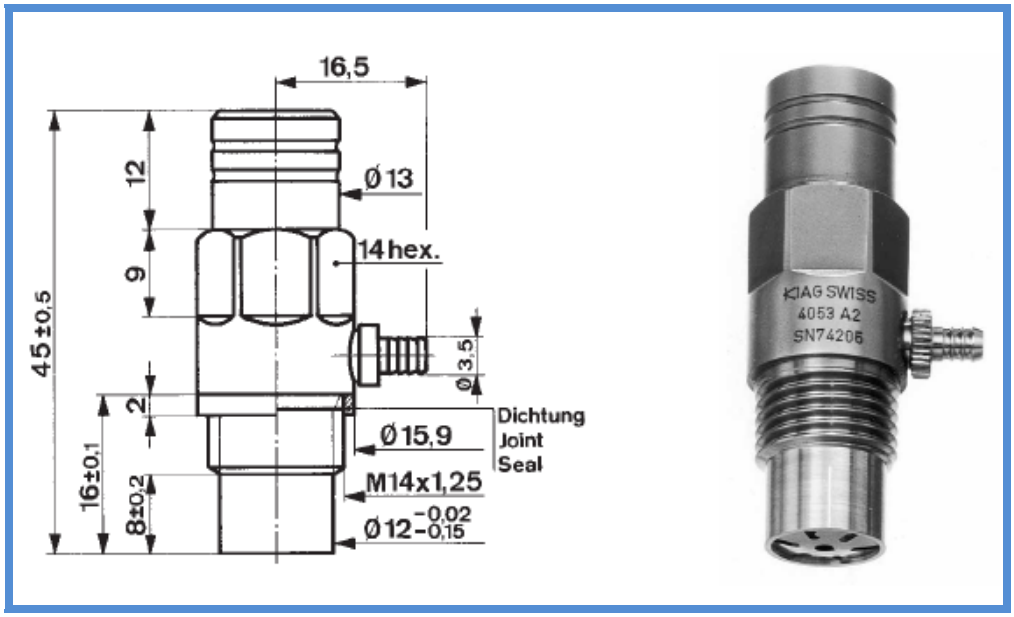

Figure 2.10 Kistler pressure sensor dimensions (Kistler 4053A specifications data sheet).

Each sensor was designed to be supplied with a constant current which was provided by an accompanying Kistler amplifier type 4618A0.

Calibration was required in order to be able to convert the voltage output from the sensor into units of pressure (Pa) and to confirm linearity. The pressure sensors were originally calibrated for use with a computer equipped with a National Instruments 5112 (PCI) data acquisition board and custom LabVIEW data acquisition software. However, the sensors were re-calibrated and used with a different computer which was equipped with a National Instruments 6259 (USB) data acquisition board and customized LabVIEW SignalExpress (v3.0) data acquisition software. The latter data acquisition system was selected for the experiment because of technical inadequacies in the former.

As with the BIV camera triggering, the National Instruments 6259 (USB) DAQ board was connected to receive the trigger signal directly from the LabVIEW signal driver program via the National Instruments AT-MIO-16E-2 DAQ board. This trigger signal started the pressure data acquisition.

Caution was required during the calibration of the sensors to avoid exceeding the pressure measurement limit (1 bar ≈ 10 m h.o.w.). Hence, in advance of performing the calibration knowledge of the maximum pressure possible with the breaking wave was required. Table 2.1 details some of the information gathered from the results of experiments conducted by several researchers. This information helped to confirm that the 4053A sensors were applicable for use. In all of the small-scale laboratory experiments referenced the maximum pressure reported never exceeded 1 bar (10^5 Pa); more so when the wave height used was less than 10 cm.

Table 2.1

Typical wave pressures from previous researchers

Reference/comments	Wave Height (m)	Period (s)	Pressure
Chen et al. (2007)	0.08	1.20	0.5 kPa
Bird et al. (1998) which referred to:			
- Walkden et al. (1995) (large scale laboratory tests, regular waves)	1.10	-	480 kPa
- Kirkgoz (1995)	"obtained peak pressures of nearly 100 times the wave height"		
Lugni et al. (2006)	0.22	-	50 kPa
Blackmore and Hewson (1984):			
- maximum pressure	0.90	4.30	48.9 kPa
- maximum pressure from smallest wave height	0.80	3.22	11.4 kPa
Whillock (1987)	varied	1-2	"140 cm h.o.w." = 14 kPa
Kamel (1970) - plate drop test	-	-	"3.8 kg/cm^2" = 372.7 kPa
Bullock et al. (2001) - laboratory drop tests (in seawater & freshwater) & full-scale wave impacts on a breakwater in Atlantic Ocean	"gauge pressure 20 kPa, typical of values in drop tests & gauge pressure 200 kPa, typical of storm-wave impacts in the field"		
Bullock et al. (2007)	1.35	8.00	>> 1 bar

The calibration was performed under hydrostatic pressures to a maximum pressure of about 30 kPa (≈ 3 m h.o.w.). During calibration the sensor was kept under appropriate hydrostatic pressure while the output data was recorded at a rate of 10 kHz for 10 s; this was done for a minimum of three attempts to attain the average output

voltage from the sensor which would then correspond to the applied hydrostatic pressure. Tabulated calibration data can be found in table 2.2 and figure 2.11 provides a graphical illustration of the calibration data. Figure 2.11 clearly illustrates the linear response of the sensor to changes in pressure. Linear regression analysis of the calibration data produced the equation y = 9911.1x - 1571.7 which was used to relate the output voltage from the sensor (x) to pressure (y) with a percentage error in the reading of 2.7%.

Work of several researchers has led to the obvious conclusion that sampling frequency has a direct effect on the data obtained when measuring dynamic parameters such as pressure. Based on the work of previous researchers who also observed breaking waves, including Schmidt et al. (1992) and Lugni et al. (2006), the sampling rate used to acquire pressure data throughout the experiment was set at 10 kHz.

Table 2.2

Pressure sensor calibration data

	Water Depth (m)	Hydrostatic Pressure (Pa)	Output Voltage (v)
1	sensor in air	0.000	0.164
2	0.133	1304.730	0.286
3	0.260	2550.600	0.431
4	0.277	2717.370	0.449
5	0.395	3874.950	0.544
6	0.564	5532.840	0.687
7	1.000	9810.000	1.147
8	2.000	19620.000	2.139
9	3.000	29430.000	3.131

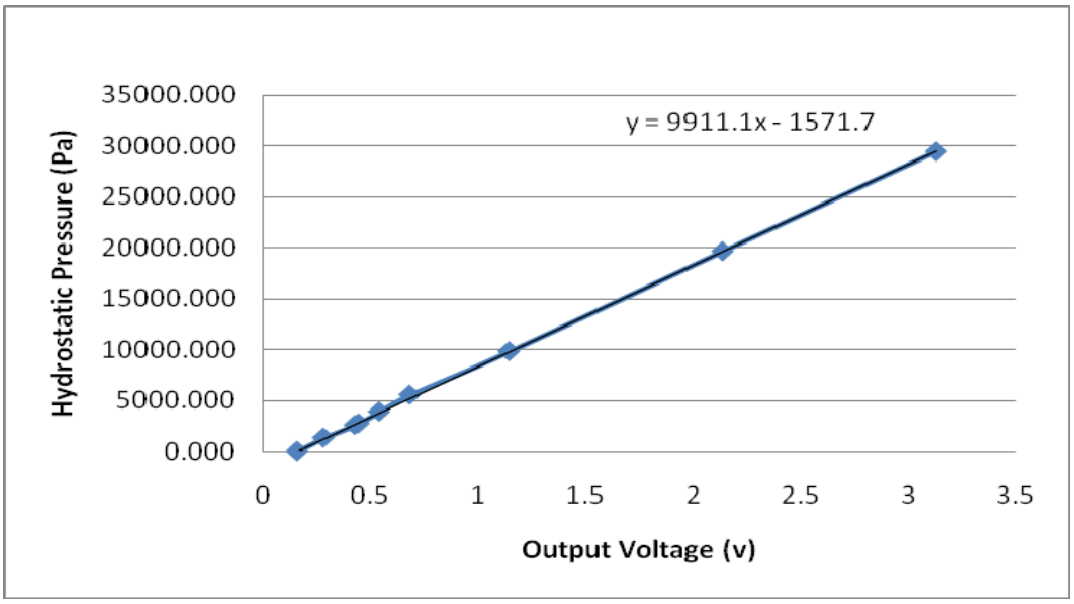

Figure 2.11 Graph of pressure sensor calibration data.

CHAPTER III

DISCUSSION OF RESULTS

Description of breaking wave

In order to study the hydrodynamics of the turbulent bore and structure interaction the experiment focused on the singular case of a plunging breaking wave forming a well developed turbulent bore. A description of the formation of a turbulent bore can be found in Ting and Kirby (1995) with overt detail.

Inspection of the resulting movies from the BIV process offered a reliable means for a proper description of the flow and its evolution; this was also useful for comparison with the findings of other researchers. In addition, the movies provide a unique means of observing the inherent air-water mixing leading up to the impact on the structure.

The evolution of the breaking wave was distinguished by an almost vertical, advancing wave front in which the crest curled over and plunged into the water ahead of the wave. The water level at the model structure was observed to remain below the still water level until the impact (that is until contact with water in the leading edge of the wave). The leading edge of the wave was formed by a protruding jet of water which was generated by the crest curling over and plunging into the water ahead of the wave. The curling over of the crest also led to a significant amount of air becoming entrapped within the wave.

At the moment of impact a "flip through" event was observed at the model structure. A flip through is a typical occurrence at the location of sea walls or coastal structures with vertical faces. The event is characterized by the body of the wave advancing with the water level at the toe of the wave (in front of the structure) rapidly moving upwards, the uprising water meeting the wave crest and forming a fast moving vertical jet of water. There is often a discrepancy between the definition of the flip through event by several researchers; for instance Hull and Muller (2002) claimed that there is no air entrapment during the event in contrast to the description provided by Lugni et al. (2006). Peregrine (2003) described the flip through process as the water level at the structure rapidly increasing, the trough of the wave fills up and the "free surface moves as if converging toward a point." Figure 3.1 and figure 3.2 display the sequence of flow and formation of the upward moving jet of water associated with the flip through event.

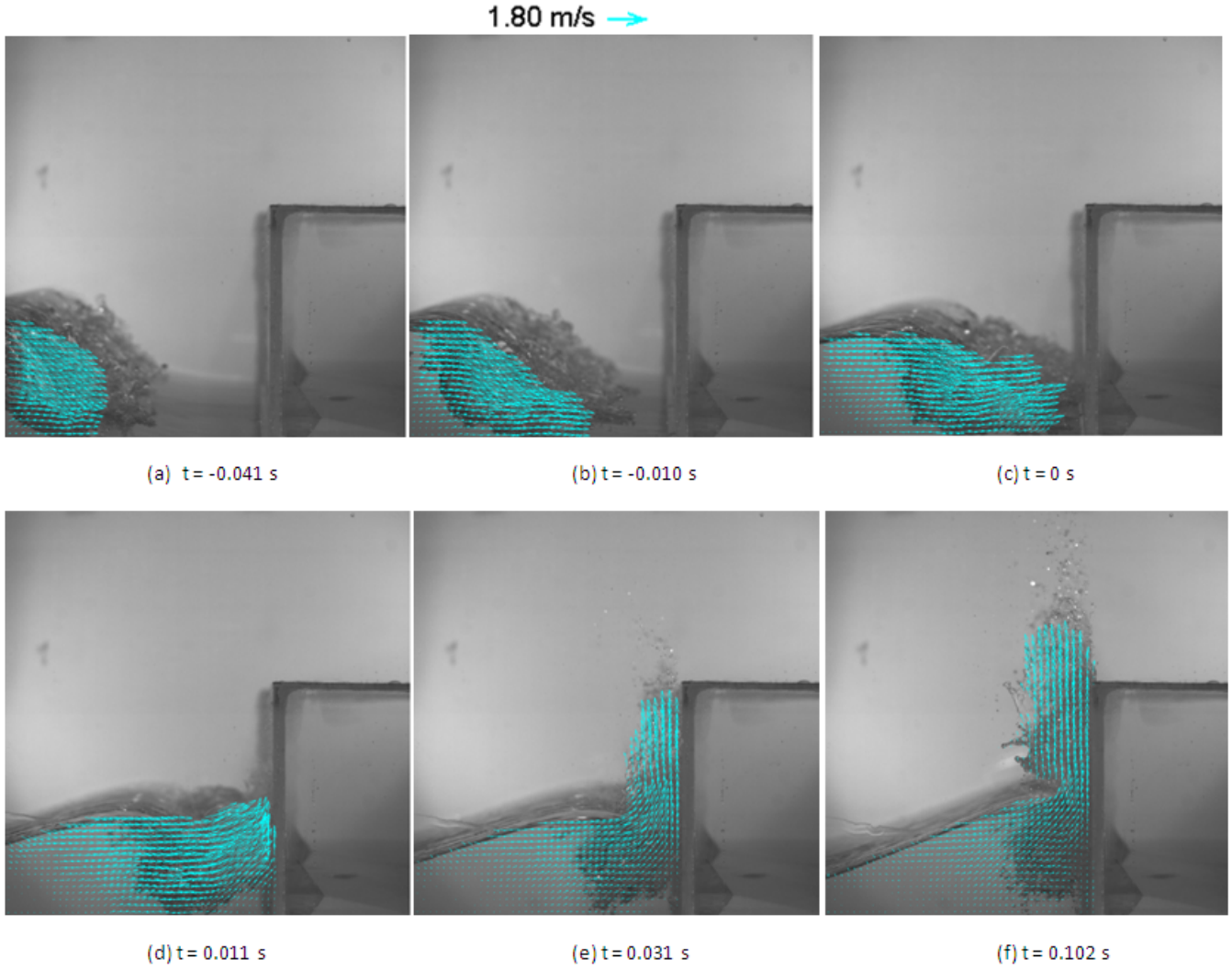

Figure 3.1 Sequence of flow leading to flip through event.

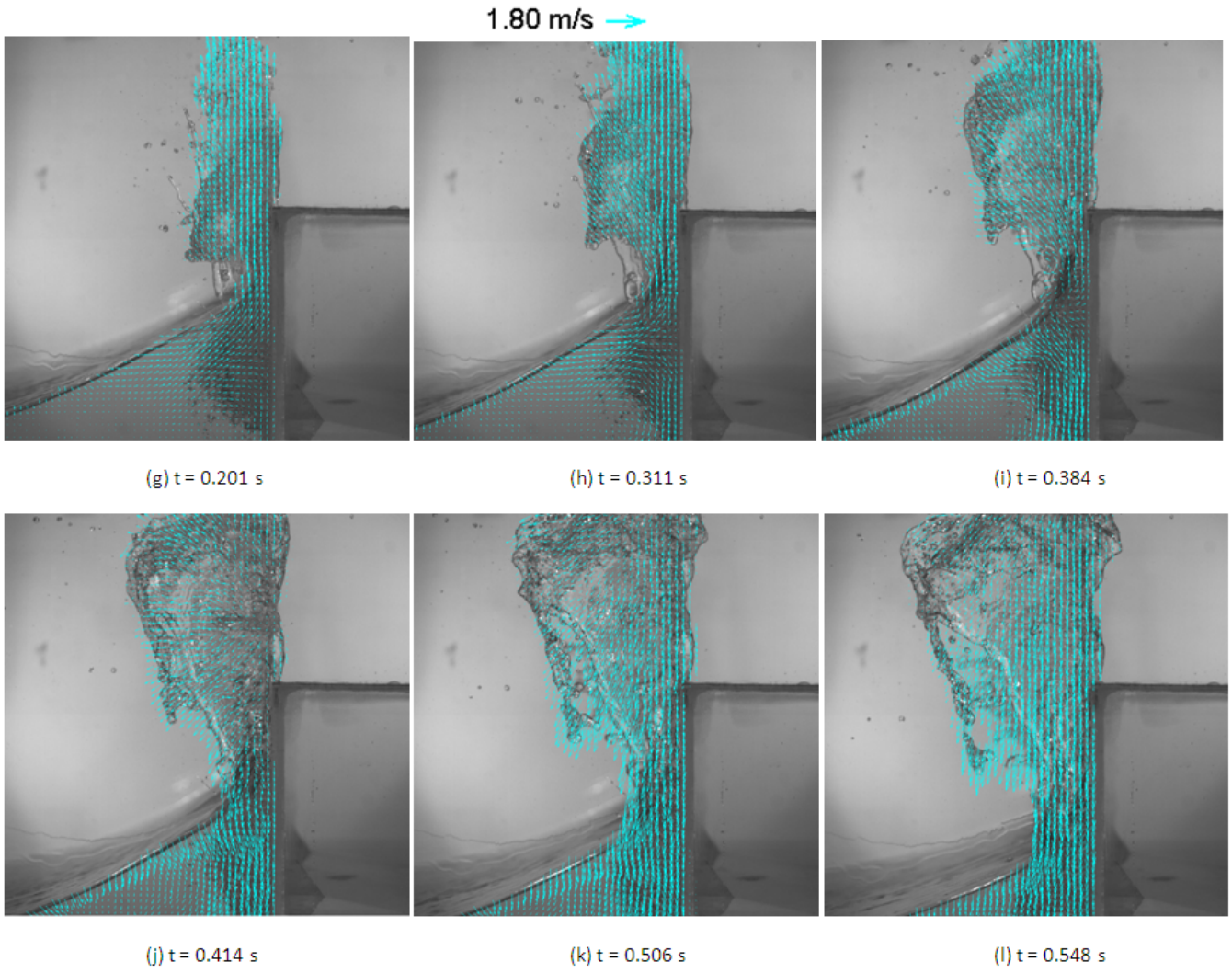

Figure 3.2 Sequence of flow after flip through event.

The general observation at the face of the model structure was as follows: forward motion was translated to vertical motion which continued upwards constrained by the structure (figure 3.1: a-f). The upward moving water was observed to continue vertically when passing the top of the structure (figure 3.2: g-i). During the experiment significantly less overtopping occurred than was expected. This was observed as a small amount of water would advance onto the top of the structure while dropping back downwards but this amount was significantly less than that which was reflected (off of the structure) and dropped back down onto the wave (figure 3.2: j-l).

The duration of the impact event was 600 ms on average. A typical wave impact event from the experiment is provided as a movie in *.avi format in Appendix A.

Velocity

By identifying the coordinates (in pixels) of the particular positions of interest (namely A, B & C; refer to figure 2.9 in Chapter II) from the BIV movies the (temporal) velocity data for these positions was extracted from the velocity field data. This facilitated comparison of velocity data with pressure data which was obtained at those same positions. Ensemble averaged velocity field data was obtained by the BIV process from a minimum of thirty test waves. Velocity data was obtained within the water just in front of the wall (approximately 4 mm away). The coordinates of the velocity data positions are listed in Table 3.1, the wall was located at x = 670 pixels.

Table 3.1

Coordinates of velocity data

	Coordinates (pixels)	
Position	x	y
A	660	759
B	660	854
C	660	949

The data confirmed that the velocities experienced at the wall were predominantly in the vertical direction during the wave impact, as was expected. Horizontal velocities experienced were evidently during the approach of the wave. A "transition point" signifying the flip through event can be identified on the plots of temporal horizontal and vertical velocity data (refer to figure 3.3 which is from the data for position A). This "transition point" can be thought of as the moment when all horizontal motion during the approach of the wave was translated to vertical motion which continued upwards constrained by the wall face.

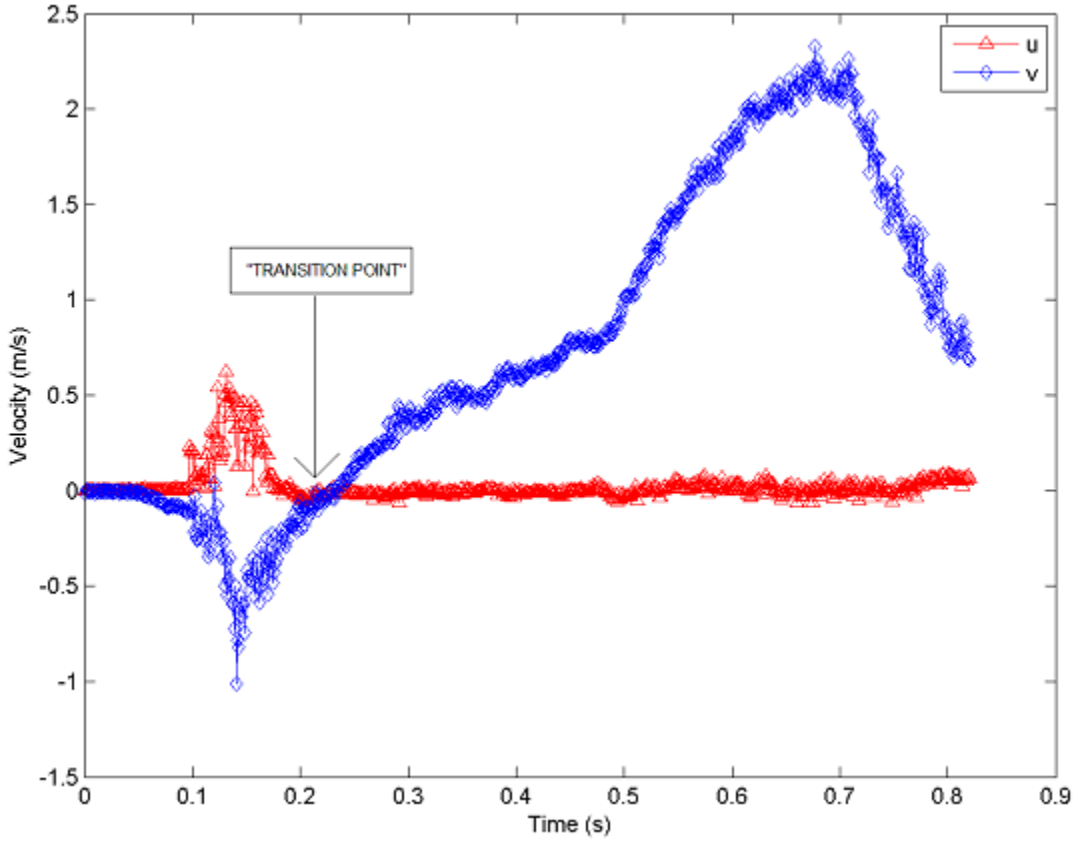

Figure 3.3 Velocity transition point.

It would be erroneous to consider the point of maximum vertical velocity to be at the moment when the water reaches its highest point just before dropping back down. Rather, bearing in mind the location of the positions (A, B & C), it is evident that subsequent to the start of the flip through event the weight of the water in the wave as it continues forward, pushes more water into the vertical jet to the point where it reaches a maximum vertical velocity. This velocity then diminishes as the jet dies and then the water drops back down. Table 3.2 provides the collated velocity data for each position.

Figure 3.4 presents a plot of the vertical velocities vs. time and figure 3.5 presents a plot of the horizontal velocities vs. time.

Table 3.2

Velocity data

		A	B	C
mean u (x 10^{-2} m/s)		1.83	2.19	2.90
mean v (m/s)		0.40	0.54	0.78
max. u	(m/s)	0.30	0.50	0.60
	(C)	0.14	0.23	0.27
max. v	(m/s)	1.90	1.80	2.30
	(C)	0.86	0.82	1.05

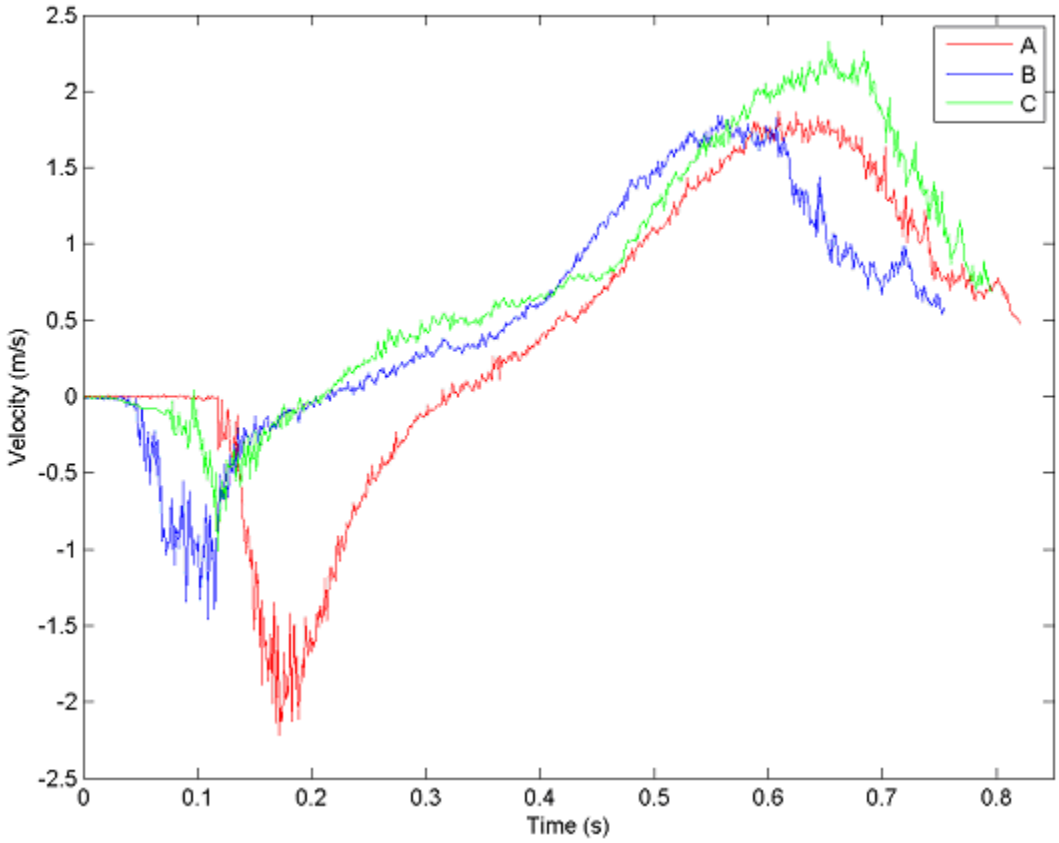

Figure 3.4 Ensemble averaged vertical velocities.

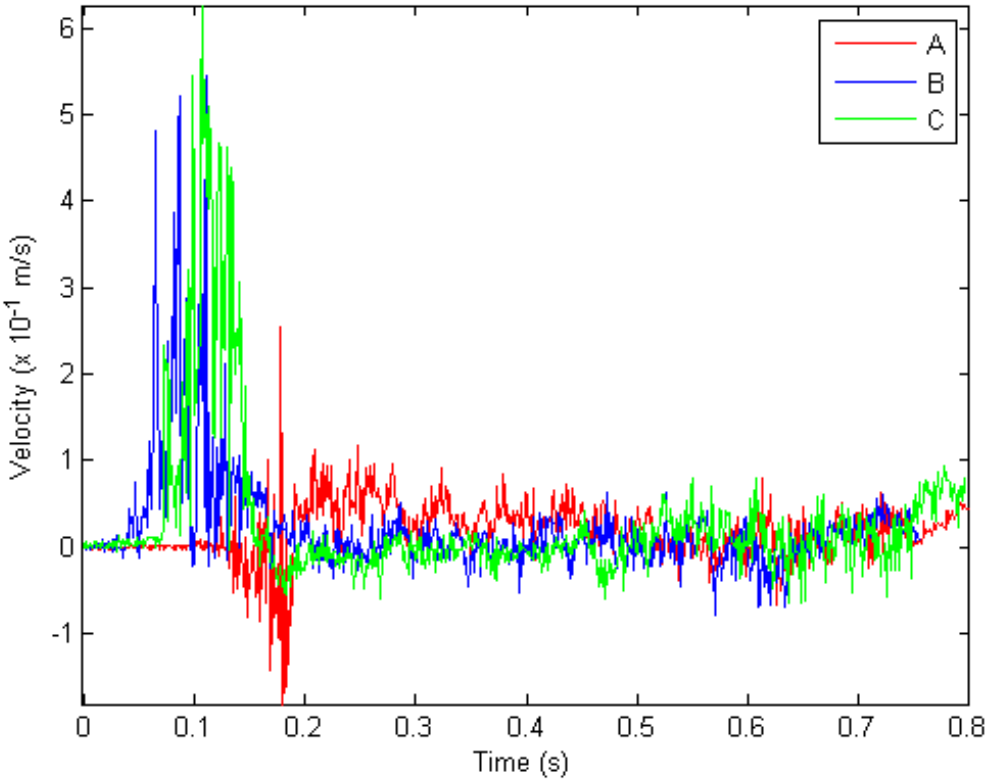

Figure 3.5 Ensemble averaged horizontal velocities.

Pressure

Mean pressure data was obtained from the ensemble averaging of the data from ten test waves for three different locations. The pressure data obtained from the experiment was interpreted considering that most violent wave impacts highly depend on the shape of the incident wave just before impact. In this case, of a turbulent bore and structure interaction the impact pressure was initiated by the water of the protruding front of the breaking wave making contact with the pressure sensors. This is reflected in

the time lapse for the start of the impact (i.e. the initial rise of pressures) for each position (A, B & C). As expected the lower positions were the first to experience the effects of the wave.

The majority of field and laboratory results from various researchers (including Bullock et al. 2001, Peregrine 2003, and Lugni et al. 2006 amongst others) present temporal pressure data which contains a distinguishable high spiked, "church-roof" shape (attributed to the initial shock pressure of the wave impact) and trailing fluctuations in pressure (attributed to air compression and/or "reflective pressure"). Most of these works focused on a plunging breaker wave shape which directly impinged onto the structure and entailed very high frequency data acquisition. Resulting pressure data in the present case contained two blunt spikes as opposed to the "church-roof" (high spike) shape seen in those results. Figures 3.6, 3.7 and 3.8 describe the formation of the resulting pressure data.

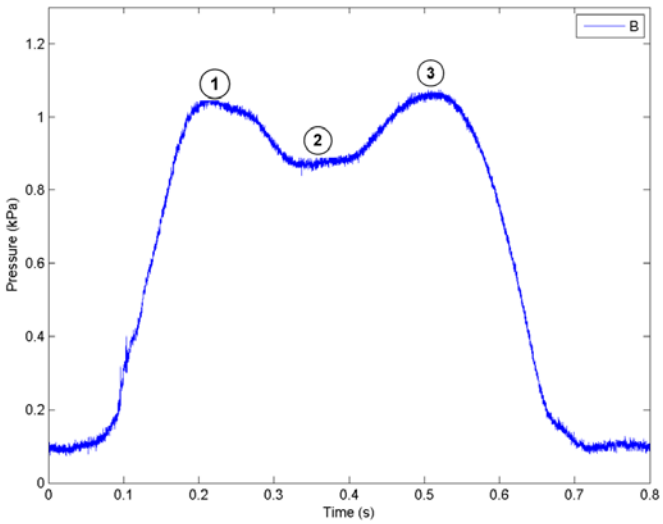

Figure 3.6 Pressure data.

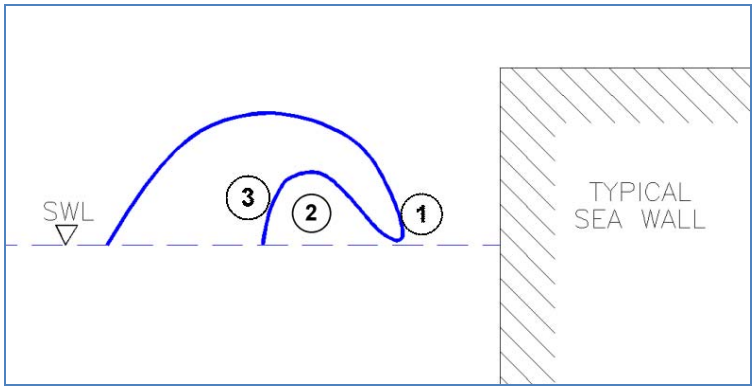

Figure 3.7 Cause of pressure data schematic.

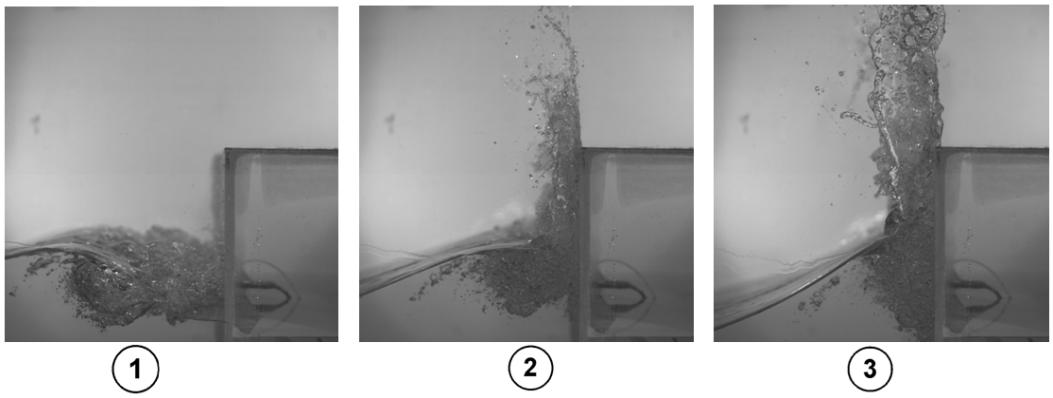

Figure 3.8 Pressure data formation images.

The shape of the resulting pressure data can be attributed to the following (refer to figures 3.6, 3.7 and 3.8): firstly (1), to the initial impact of the protruding jet of the breaking wave which causes the first maxima, secondly (2), to the sensor encountering the bulk of the entrapped air hence causing the drop in pressure between the blunt spikes and lastly (3), to the inherent hydrostatic pressure combined with the compression of the entrapped air bubbles, by the subsequent forward motion of the water within the wave,

which causes the second maxima. The point of maximum pressure was found to always be within the second maxima. Further investigation and equipment would be necessary in order to determine the inherent effects and magnitude of "reflective pressures." Figure 3.9 displays the pressure data for each position and figures 3.10, 3.11 and 3.12 provide comparisons of the pressure data with the velocities for each position.

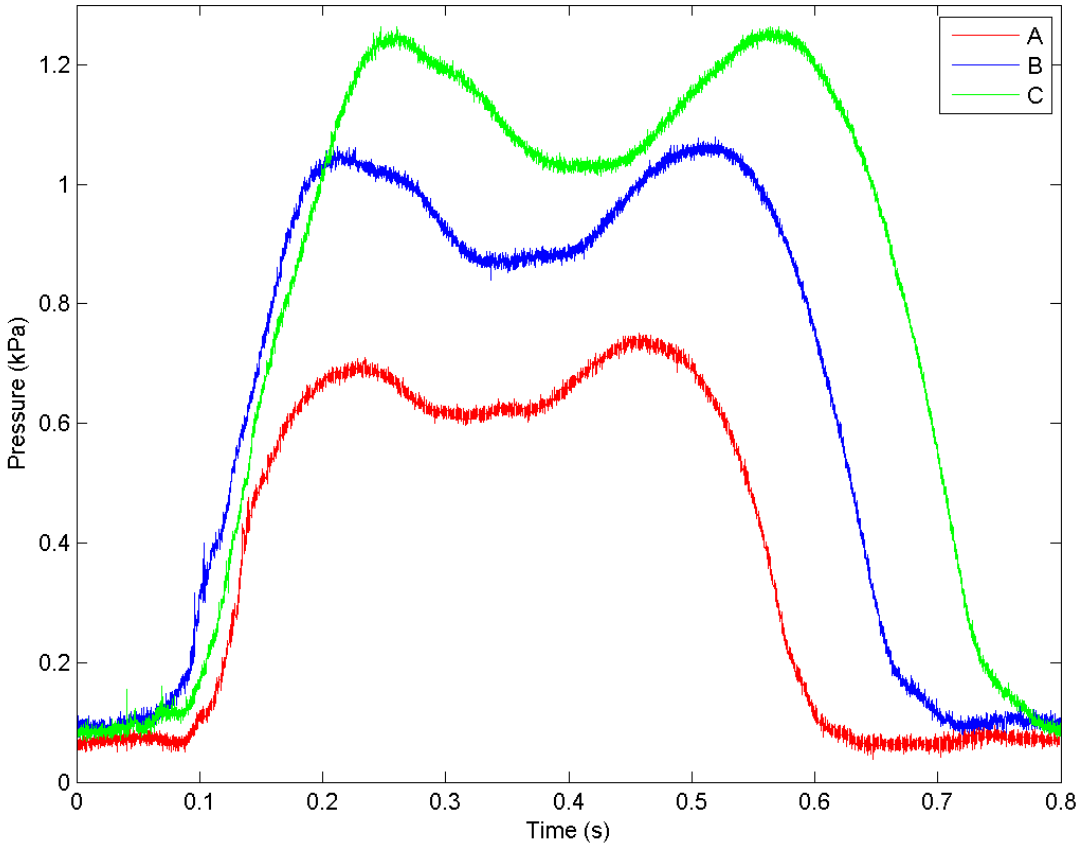

Figure 3.9 Ensemble averaged pressure data for each position.

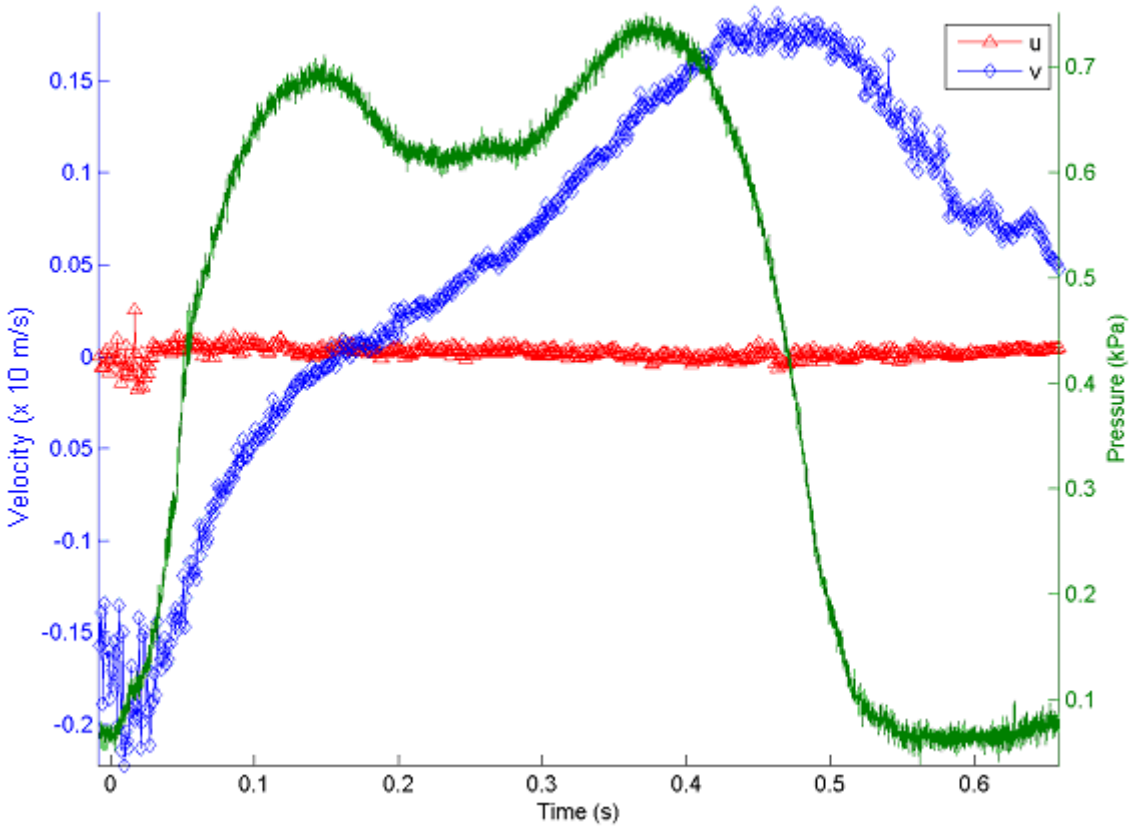

Figure 3.10 Ensemble averaged pressure and velocity for position A.

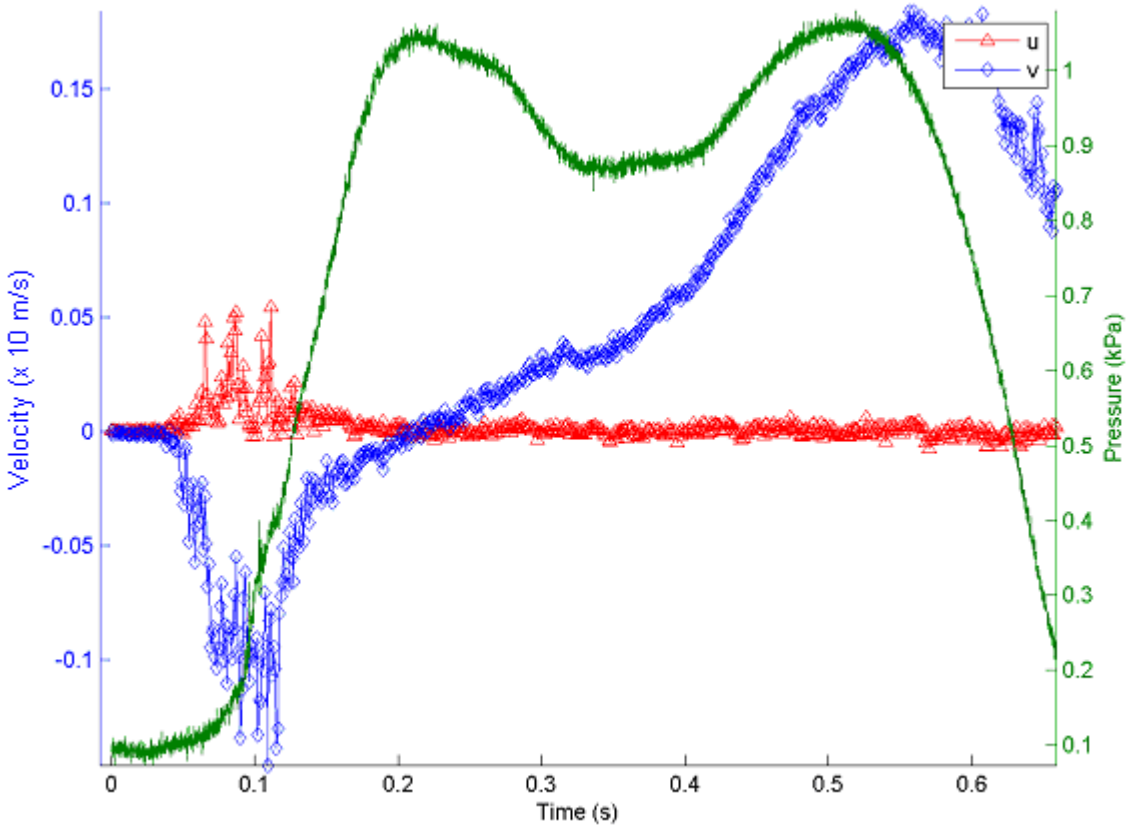

Figure 3.11 Ensemble averaged pressure and velocity for position B.

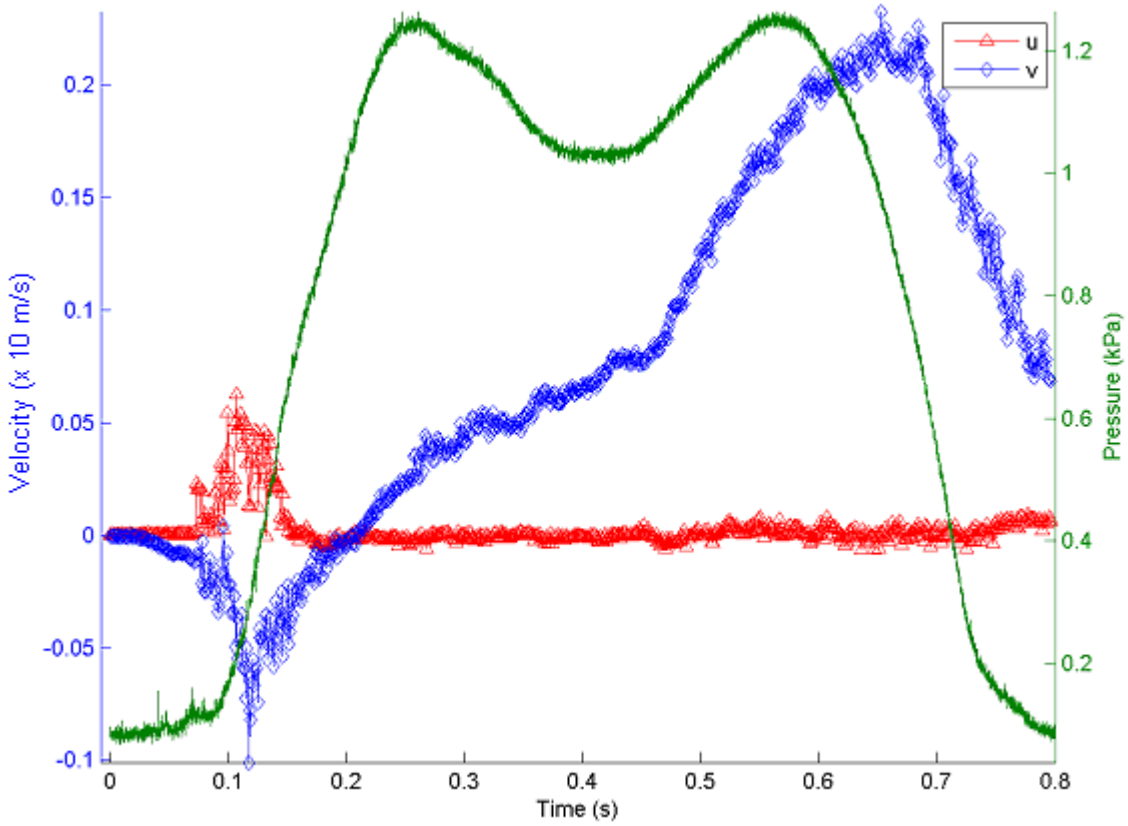

Figure 3.12 Ensemble averaged pressure and velocity for position C.

The compression of the air entrapped within the wave is a well-established and observed secondary phenomenon. Lugni et al. (2006) provides an explicit description of the pressure induced by a wave and of the inherent components which contribute to the overall pressure; he attributed secondary pressures to reflection, air compression and interestingly, also to "the sudden vertical acceleration of the flow which induces a high local pressure during a very short time interval." Peregrine (2003) also found similar results of high pressures related to the vertical acceleration of the flow at the wall.

Careful observation of the BIV movies and synchronized data illustrated in figures 3.10, 3.11 and 3.12 led to the conclusion that in the present case of the turbulent bore-structure interaction the consequential maximum pressure was a direct result of the compression of the entrapped air by the weight of the water in the wave as it continued forward onto the structure. Furthermore, comparing the time of occurrence of the maximum pressures with the corresponding frames of the BIV movies led to the observation that the maximum pressure occurred at the moment when the entrapped air pocket or rather the bulk of the group of entrapped air bubbles was directly at the pressure sensor position. Figure 3.13 shows the frames extracted from the BIV movies which correspond to the times of maximum pressure for each position.

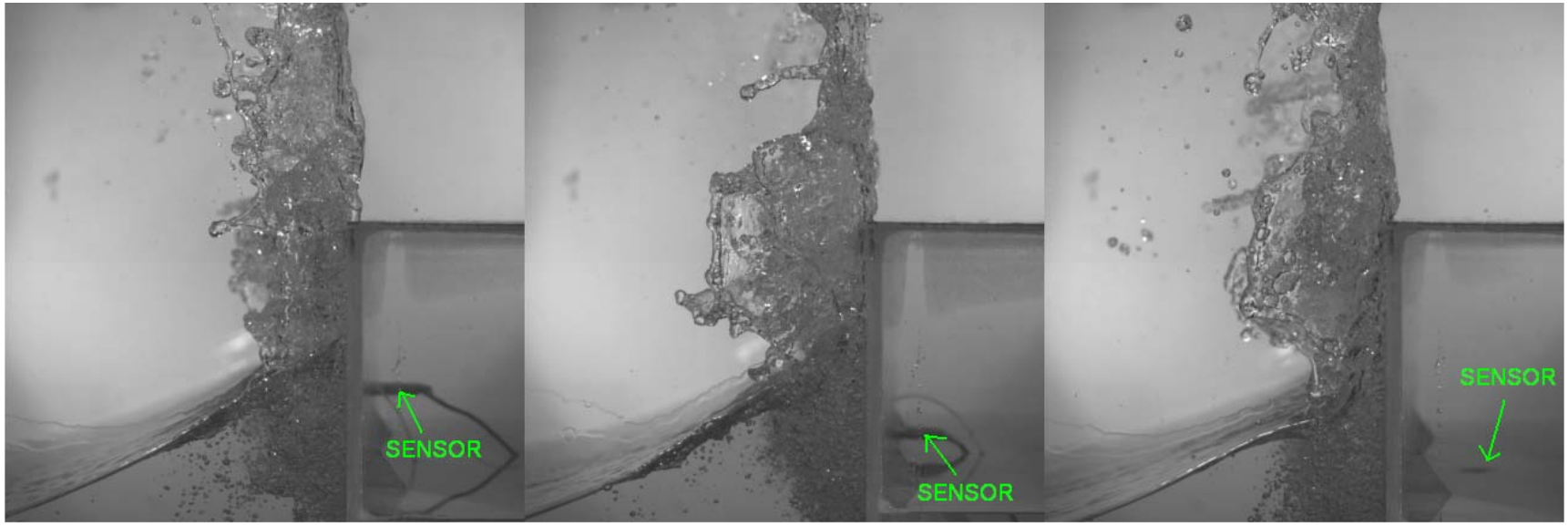

Figure 3.13 BIV movie frames at maximum pressure.

Extensive research work has confirmed the form of the vertical pressure distribution at a sea wall. According to Peregrine (2003) "once the point of maximum pressure is known, the pressure field has a simple pattern, which decays with distance from the maximum to near hydrostatic pressures." In accordance with theoretical expectations the location of maximum pressure in the experiment was found to occur just below the SWL at position C.

As in Lugni et al. (2006) for practical purposes the pressure exerted on the structure was expressed in terms of its integral with respect to time for the duration of the impact event; that is the pressure impulse, P (in Pa s) as in equation 3-1:

$$P = \int_{t_0}^{t_1} p\,dt \qquad (3\text{-}1)$$

In which p is the pressure in Pascals and t_0 and t_1 are, respectively, the times before and after impact. Peregrine (2003) also used the pressure impulse to signify the pressures of the impact event. It should be noted that their calculation was limited to the extremely short duration of the impact of the wave which, according to their results, typically occurred within 4 to 8 milli-seconds. By considering only this very short impact time their calculations do not consider the total time of the impact event at the wall and the inherent components which contribute to the overall pressure which may be more significant for coastal structure design. The pressure impulse for the present experiment was calculated for the entire duration of the impact event. Tabulated pressure and pressure impulse data can be found in table 3.3.

Table 3.3

Pressure data

		A	B	C
max. pressure	(kPa)	0.75	1.07	1.27
	$p/(\frac{1}{2}\rho C^2)$	0.31	0.44	0.53
pressure impulse (kPa s)		0.33	0.51	0.65

Inspection of the vertical velocities subsequent to the "flip-through" event (i.e. after the formation of the upward moving jet) revealed that acceleration of the motion of the water was 1.5 g. Figure 3.14 shows a sample of the vertical velocity data used to calculate acceleration.

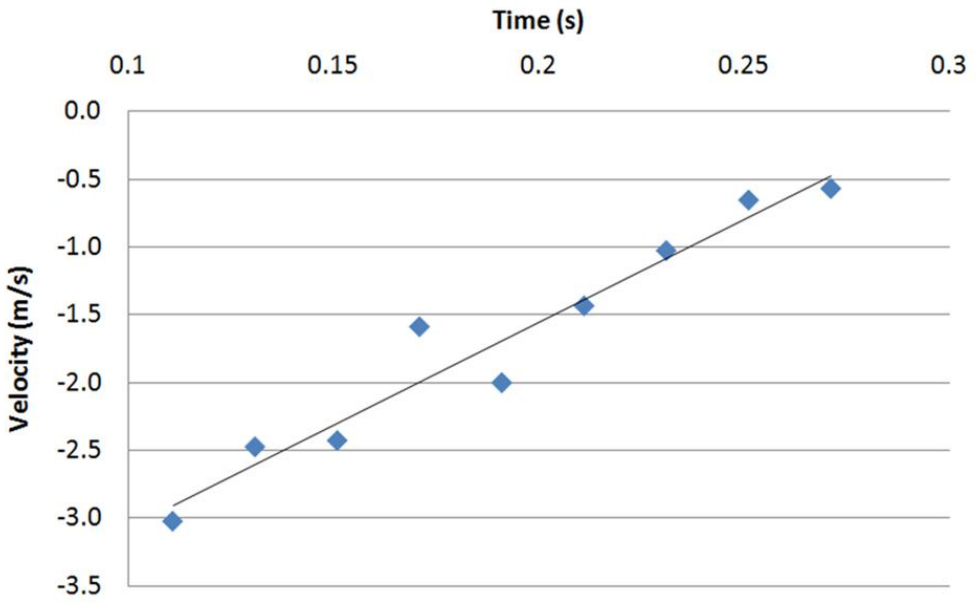

Figure 3.14 Vertical acceleration.

Figures 3.15, 3.16 and 3.17 present the non-dimensionalised pressure and velocity data. P^d denotes non-dimensionalised pressure: $p/(½\rho C^2)$. Non-dimensionalised time, t/T, is denoted by: t^d. 1000 kg/m^3 was used as the density of water (ρ). Table 3.4 presents dimensionless max. pressure data from the results of other researchers, calculated based on the wave parameters and pressure data from each case.

Table 3.4

Dimensionless pressure data

	Dimensionless pressure $p/(\frac{1}{2}\rho C^2)$
Whillock (1987)	35.68
Chen et al. (2007)	0.25
Bullock et al. (2007)	55.62
Bullock et al. (2007) [a]	16.31

[a] for broken wave impact case similar to this experiment

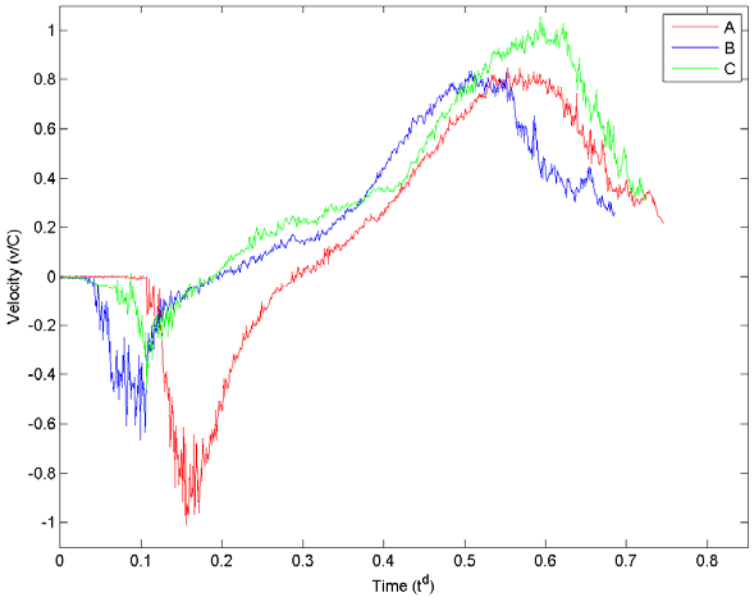

Figure 3.15 Non-dimensionalised vertical velocity.

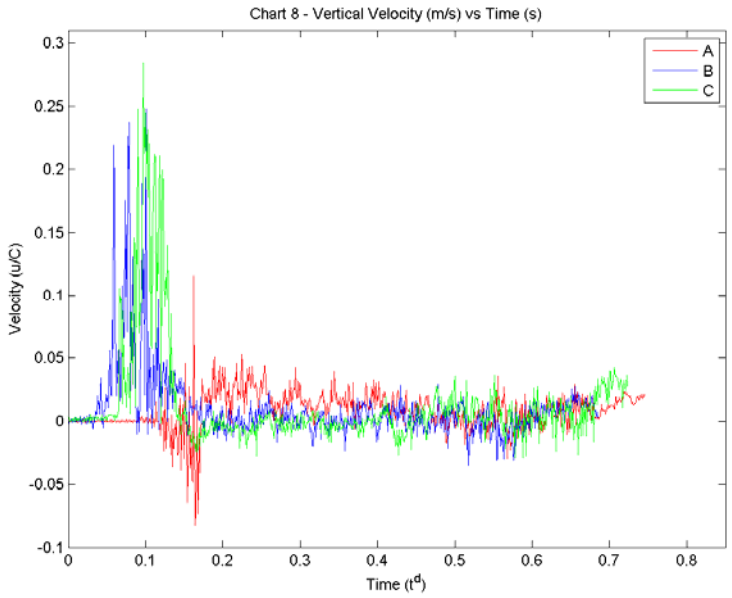

Figure 3.16 Non-dimensionalised horizontal velocity.

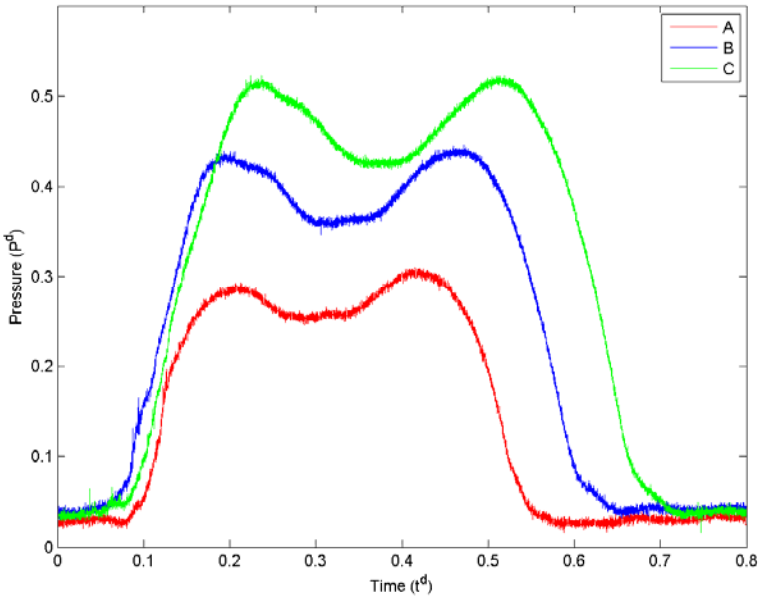

Figure 3.17 Non-dimensionalised pressure data.

Limitations of results

Comparison of the pressure data obtained with calculations based on well-known pressure formulas such as in the Goda, Sainflou and/or Minikin methods would be interesting, but would however provide inaccurate results without any precise void fraction (air/water ratio) data. The pressure formulas presented in these methods all provide good estimates for maximum pressures for most wave cases. However, the results tend to be overestimated approximations of pressure based on an estimated overall hydrostatic pressure associated with a particular (design) wave height at the wall at the moment of impact; much like in the "simplistic" depth-limited design method which was proven to be flawed by Kamphuis (2000).

Void fraction data would be necessary to determine the exact wave height at the point of impact and also for an accurate measure of the density of the air-water mixture. The Sainflou method which makes the assumption that there is water at SWL at the back face of the structure (i.e. the side adjacent to the wave approach) may be more applicable for the present set-up.

CHAPTER IV

CONCLUSION

Summary

The hydrodynamics of a coastal structure-turbulent bore interaction was studied by examination (two-dimensional) of the singular case of a plunging breaking wave forming a well developed turbulent bore which impacted on a model sea wall structure.

The turbulent bore impact event was found to display similar characteristics to the impact event of other wave shapes, in particular that of a plunging breaker. Examination of the impact event confirmed the conversion of nearly all horizontal velocity to vertical velocity during the "flip through" event.

In accordance with theoretical expectations the location of maximum pressure was found to occur just below the SWL.

Resulting pressure data in the present study consisted of two blunt spikes as opposed to the "church-roof" (high spike) shape seen in other results. The shape of the pressure data was attributed to the following: firstly, to the initial impact of the protruding jet of the breaking wave which causes the first maxima, secondly, to the sensor encountering the bulk of the entrapped air hence causing the drop in pressure between the blunt spikes and lastly, to the inherent hydrostatic pressure combined with the compression of the entrapped air bubbles, by the subsequent forward motion of the

water within the wave, which causes the second maxima. The point of maximum pressure was found to always be within the second maxima.

Observation of the turbulent bore-structure interaction showed that the consequential maximum pressure was a direct result of the compression of entrapped air by the weight of the water in the wave as it continued forward onto the structure combined with the inherent hydrostatic pressure of the wave.

Scope for future work

Measurement of the amount of entrapped air within a breaking wave would be possible by use of Fiber Optic Reflectometer (FOR) equipment. The FOR equipment would provide an innovative method for measuring the amount of entrapped air by void fraction measurement (air/water ratio) within a breaking wave. The data would help to determine the exact wave height at the point of impact and also give an accurate measure of the density of the air-water mixture in the breaking wave.

By design the FOR system can be considered a non-intrusive measurement method as there will be minimal interference with the breaking wave phenomenon. More information on the FOR system is available from the developers in their publication (Chang et al. 2003).

The data obtained from the use of the FOR system would ultimately help to determine the relationship between (dynamic & hydrostatic) pressure, velocity and the

amount of entrapped air of breaking waves and confirm how these factors affect the overall (dynamic) force of the wave.

REFERENCES

Bird, P.A.D., Crawford, A.R., Hewson, P.J., Bullock, G.N., 1998. An instrument for field measurement of wave impact pressures and seawater aeration. Coastal Engineering 35, 103–122.

Blackmore, P.A., Hewson, P.J., 1984. Experiments on full-scale wave impact pressures. Coastal Engineering, 8, 331-346.

Bullock, G.N., Crawford, A.R., Hewson, P.J., Walkden, M.J.D., Bird, P.A.D., 2001. The influence of air and scale on wave impact pressures. Coastal Engineering 42 (4), 291–312.

Bullock, G.N., Obhrai, C., Peregrine, D.H., Bredmose, H., 2007. Violent breaking wave impacts. Part 1: Results from large-scale regular wave tests on vertical and sloping walls. Coastal Engineering 54, 602–617.

Chang, K.-A., Lim, H., Chin, B.S., 2003. Fiber optic reflectometer for velocity and fraction ratio measurements in multiphase flows. Review of Scientific Instruments 74 (7), 3559-3565.

Chen, X., Li, Y., Teng, B., 2007. Numerical and simplified methods for the calculation of the total horizontal wave force on a perforated caisson with a top cover. Coastal Engineering 54, 67–75.

Dean, R.G., Dalrymple, R.A., 1992. Water wave mechanics for engineers and scientists. Second edition. World Scientific Publications, Singapore.

Hattori, M., Arami, A., 1992. Impact breaking wave pressures on vertical walls. Proceedings of 23rd ICCE, ASCE, 2, Venice, Italy, pp. 1785-1798.

Hattori, M., Arami, A., and Yui, T., 1994. Wave impact pressure on vertical wall under breaking waves of various types. Coastal Engineering 22, 79-114.

Hull, P., Muller, G., 2002. An investigation of breaker heights, shapes and pressures. Ocean Engineering 29, 59–79.

Kamel, A.M., 1970. Shock pressure on coastal structures. J. Waterways, Harbors & Coastal Eng. Div. ASCE 7687 (WW3), 689-699.

Kamphuis, J.W., 2000. Introduction to coastal engineering and management. World Scientific Publishing Co. Pte. Ltd., Singapore.

Kirkgöz, M.S., 1995. Breaking wave impact on vertical and sloping coastal structures. Ocean Engineering, 22, 35-48.

La Vision, 2000. PIV Flow Master Manual. Gottingen, Germany: La Vision GmbH.

Lugni, C., Brocchini, M., Faltinsen, O.M., 2006. Wave impact loads: the role of the flip-through. Physics of Fluids 18, 122101, 1-17.

Maxwell, J.C., 1892. A treatise on electricity and magnetism. Oxford: Clarendon Press.

Minikin, R.R., 1963. Wind, waves and maritime structures. London: Griffin.

Mori, N., Chang, K.-A., 2003. Introduction to MPIV. User manual and program available online at http://www.oceanwave.jp/softwares/mpiv/

Peregrine, D.H., Topliss, M.E., Cooker, M.J., 1992. Pressure oscillations during wave impact on vertical walls. Proceedings of 23rd ICCE, ASCE, 2, Venice, Italy, pp. 1639-1650.

Peregrine, D.H., Topliss M.E., 1994. The pressure field due to steep water waves incident on a vertical wall. Proceedings of 24th ICCE, ASCE, 2, Kobe, Japan, pp. 1496-1510.

Peregrine, D.H., 2003. Water-wave impact on walls. Annu. Rev. Fluid Mech. 35, 23–43.

Ryu Y., 2006. Extreme wave impinging and overtopping. Ph. D. dissertation. Texas A&M University, College Station, TX.

Ryu, Y., Chang, K.-A., 2008. Green water void fraction due to breaking wave impinging and overtopping. Exp. Fluids 45, 883–898.

Ryu Y., Chang, K.-A., Lim, H.-J., 2005. Use of bubble image velocimetry for measurement of plunging wave impinging on structure and associated greenwater. Meas. Sci. Technol. 16:1945–1953.

Schmidt, R., Oumeraci, H., Partensky, H.W., 1992. Impact loads induced by plunging breakers on vertical structures. Proceedings of 23rd ICCE, ASCE, 2, Venice, Italy, pp. 1545-1558.

Seol, D.-G., Bhaumik, T., Bergmann, C., Socolofsky, S.A., 2007. Particle image velocimetry measurements of the mean flow characteristics in a bubble plume. Journal of Engineering Mechanics 133, 665-676.

Ting, F.C.K., Kirby, J.T., 1995. Dynamics of surf-zone turbulence in a strong plunging breaker. Coastal Engineering 24, 177-204.

Walkden, M.J.A., Crawford, A.R., Bullock, G.N., Hewson, P.J., Bird, P.A.D., 1995. Wave impact loading on vertical structures. Proceedings of ICCSB 1995, ICE, London, pp. 273–286.

Whillock, A.F., 1987. Measurements of forces resulting from normal and oblique wave approaches to small scale sea walls. Coastal Engineering, 11, 297-308.

APPENDIX A

BIV MOVIE FILES

Appendix A contains movie files in *.avi format: movie 1 shows a typical wave impact event from the experiment, movie 2 shows the ensemble averaged velocity field data superimposed on a pre-selected instantaneous BIV movie and movie 3 shows the isolated vectors from the ensemble averaged velocity field data. This appendix accompanies this thesis as a separate file available for downloading.

VITA

Name:	Arthur L.C. Antoine
Address:	CE/TTI 802-C, 3136 TAMU, College Station, TX 77843-3136, USA
Email Address:	anto322@neo.tamu.edu
Education:	B.S., Civil Engineering, University of The West Indies, 2003